

## Conditional multi-step attribution for climate forcings

Christopher R. Wentland<sup>1</sup>, Michael Weylandt<sup>2</sup>, Laura P. Swiler<sup>3</sup>, Thomas S. Ehrmann<sup>3</sup>, Diana Bull<sup>3</sup>

<sup>1</sup> Sandia National Laboratories, Livermore, CA, USA

<sup>2</sup> Zicklin School of Business, Baruch College, CUNY, New York, NY, USA

<sup>3</sup> Sandia National Laboratories, Albuquerque, NM, USA

arXiv:2409.01396v1 [stat.AP] 2 Sep 2024

*Corresponding author:* Christopher R. Wentland, crwentl@sandia.gov

**ABSTRACT:** Attribution of climate impacts to a source forcing is critical to understanding, communicating, and addressing the effects of human influence on the climate. While standard attribution methods, such as optimal fingerprinting, have been successfully applied to long-term, widespread effects such as global surface temperature warming, they often struggle in low signal-to-noise regimes, typical of short-term climate forcings or climate variables which are loosely related to the forcing. Single-step approaches, which directly relate a source forcing and final impact, are unable to utilize additional climate information to improve attribution certainty. To address this shortcoming, this paper presents a novel multi-step attribution approach which is capable of analyzing multiple variables conditionally. A connected series of climate effects are treated as dependent, and relationships found in intermediary steps of a causal pathway are leveraged to better characterize the forcing impact. This enables attribution of the forcing level responsible for the observed impacts, while equivalent single-step approaches fail. Utilizing a scalar feature describing the forcing impact, simple forcing response models, and a conditional Bayesian formulation, this method can incorporate several causal pathways to identify the correct forcing magnitude. As an exemplar of a short-term, high-variance forcing, we demonstrate this method for the 1991 eruption of Mt. Pinatubo. Results indicate that including stratospheric and surface temperature and radiative flux measurements increases attribution certainty compared to analyses derived solely from temperature measurements. This framework has potential to improve climate attribution assessments for both geoengineering projects and long-term climate change, for which standard attribution methods may fail.

## 1. Introduction

Climate impacts have broad economic (Smith and Katz 2013; Callahan and Mankin 2022), health (Luber and McGeehin 2008), political (Yamamoto and Esteban 2010), and national security ramifications (National Intelligence Council 2021). As such, the ability to robustly understand the root causes of climate impacts and quantitatively measure certainty in their outcomes is central to scientific, legal, and policy communities. Due to the chaotic nature of the climate system, detection and attribution (D&A) of a climate impact to a climate forcing is plagued by natural (or internal) variability. The further downstream, shorter duration, or more spatially-localized the change, the larger the role that variability plays. Hence, multiple climate attribution approaches (Hegerl et al. 2010) have been developed to decipher a signal from the noise, i.e., a forced response from underlying variability. In this paper we will draw upon existing climate attribution concepts to present a novel multi-step framework that achieves higher certainty attribution of downstream impacts by employing scaling experiments in a conditional Bayesian formulation.

Attribution of long-term climate impacts to anthropogenic forcings such as greenhouse gases (GHG) and aerosols in the climate system is a well-established practice (Mitchell et al. 2001; Eyring et al. 2021). These studies rely almost entirely on the “optimal fingerprinting” methodology first introduced by Hasselmann (1993) and refined over the following decade (Santer et al. 1993; Hasselmann 1997; Hegerl et al. 1997; Hegerl and North 1997; North and Stevens 1998; Allen and Stott 2003). This method determines spatial and/or temporal patterns of impacts under externally forced conditions. Typically, observational data are regressed on simulation results driven by candidate external forcings of pre-specified GHG or aerosol emission levels. The regression coefficients and corresponding significance are used to identify combinations of forcings which “best fit” the observational data; these are the important forcings to which the change is attributed. The forced simulation data might be as simple as a global average time series “signal,” though in many studies a signal is computed from the projection of data onto a set of empirical orthogonal functions (derived from a principal component analysis). A large body of work aims to identify optimal fingerprints which best improve the signal-to-noise ratio (Ribes et al. 2013), characterize and accommodate for the internal variability of the climate (Santer et al. 2011; Wills et al. 2020), and perform regional attribution studies (Bonfils et al. 2008; Stott et al. 2010). Multivariate fingerprinting approaches utilize multiple climate variables (such as temperature and precipitation

together) to identify a fingerprint which more robustly achieves attribution (Bonfils et al. 2020; Marvel et al. 2020). Bayesian formulations of the fingerprinting problem allow analysts to more deliberately quantify uncertainty in the fitted model (Hannart 2016) and encode prior knowledge of climate forcings (Berliner et al. 2000).

Pattern scaling techniques (Arnell et al. 2019; Osborn et al. 2016; Herger et al. 2015) can be used to evaluate the degree to which an external forcing (e.g., the amount of GHG) changes the magnitude of the response; these patterns are normally expressed as a change per degree of global-mean temperature change (Osborn et al. 2016). This is similar to epidemiological studies which invoke dose-response relationships as evidence of causal relationships (Hill 1965). Since the degree of GHG forcing is not contested, retrospective associative pattern attribution (Hegerl et al. 2010) studies evaluating the sensitivity of impacts to the amount of GHG forcing are not common.

“Multi-step” fingerprinting methods attempt to link downstream impacts to a climate forcing through a series of single-step fingerprinting assessments (Hegerl et al. 2010). By incorporating progressive steps of the process, this method explicitly evaluates the physical mechanism by which a driver influences a downstream impact. The assumed statistically-independent nature of the component steps unfortunately limits the confidence in such analyses to that of the single weakest attribution step. The literature appears devoid of any such multi-step attribution findings following the procedure outlined by Hegerl et al. (2010), successful or otherwise, likely due to this limitation. Other multi-step attribution frameworks exist beyond the optimal fingerprinting canon (Gonzalez et al. 2023), but remain rare.

The above attribution methods often struggle to achieve successful attribution in regimes where the forcing response is dominated by the climate’s internal variability. In particular, there are many climatic events that are short-lived and characterized by large variability in the forcing response. These can arise from spatially and/or temporally localized external forcings like forest fires (Liu et al. 2014), industrial fires (e.g., the Kuwait oil fires (Browning et al. 1992)), volcanic eruptions (Parker et al. 1996), and geoengineering projects such as marine cloud brightening or stratospheric aerosol injection (Irvine et al. 2016). The characteristic time scales of these events and their purported impacts (months or years) are much shorter than those of anthropogenic climate

change (decades), and their attribution requires methods capable of overcoming the associated low signal-to-noise ratios for the impacts of interest.

In this paper we develop a novel multi-step attribution approach for which the inclusion of additional steps can *increase* the confidence of attribution of downstream impacts from a localized source forcing. Rather than the assumed statistical independence of steps as in the method noted by Hegerl et al. (2010), this new method relies on a *conditional* Bayesian approach which leverages significant relationships in each step to increase attribution certainty. Under this formulation, stronger relationships found in intermediary steps of the causal pathway improve the ability to distinguish between different forcing levels, and confidence in attributing an observed response to a specific forcing level is increased. While we use the phrase “multi-step” to describe this method, this represents a significant departure from the approach outlined by Hegerl et al. (2010) and the two otherwise bear little resemblance.

To demonstrate the proposed methodology for a short-term climate forcing marred by high variability in the impact response, we examine the June 15th, 1991 eruption of Mt. Pinatubo. We propose several multi-step pathways (depicted in Figure 1) derived from the eruption’s injection of  $\sim 10$  teragrams of  $\text{SO}_2$  into the atmosphere and the resulting formation of sulfates in the stratosphere. These stratospheric sulfates preferentially scatter incoming solar radiation to decrease surface temperatures, while absorbing outgoing radiation from the surface to increase stratospheric temperatures. Using our novel approach, we can correctly attribute the eruption size (forcing level) based on downstream observations and increase our confidence in the attribution of the forcing level by including conditionally-dependent intermediary steps.

## **2. Case Study: Mount Pinatubo**

This section provides an overview of the eruption of Mt. Pinatubo and its impacts, and also outlines the particular set of simulations used to demonstrate multi-step attribution. Mt. Pinatubo is an attractive case study because its impacts have been well studied, allowing us to focus on demonstrating the proposed novel attribution framework and rely on known properties of the eruption response.

### *a. Impacts from Mt. Pinatubo*

Large volcanic eruptions (e.g., from Mt. Tambora, Krakatoa, Mt. Pinatubo) are a significant source of aerosol forcing in the stratosphere. The resultant impacts from aerosol forcings in the stratosphere due to explosive volcanic eruptions are as wide ranging as surface temperature decreases (Parker et al. 1996; Soden et al. 2002), lower stratosphere temperature increases (Labitzke and McCormick 1992), reduction in global precipitation (Gillett et al. 2004), lowering of global sea-level (Church et al. 2005), and increased diffusivity of incoming radiation (Robock 2000; Proctor et al. 2018) with resultant impacts on net primary productivity of plants (Gu et al. 2003; Proctor et al. 2018; Greenwald et al. 2006). The magnitude, and hence detectability and attribution, of these impacts is dependent upon the magnitude of the eruption (Marshall et al. 2019) as well as the state of the climate at time of eruption (Zanchettin et al. 2022).

As presented in Figure 1, we are concerned with the primary radiative and temperature impacts from Mt. Pinatubo. Mt. Pinatubo released 18–19 Tg of  $\text{SO}_2$  into the atmosphere (Guo et al. 2004) with only  $\sim 10$  Tg remaining in the stratosphere for further microphysical and chemical evolution into sulfate aerosols (Kremser et al. 2016). These sulfate aerosols control radiative forcing by scattering incoming shortwave radiation and absorbing longwave and near-infrared radiation (Brown et al. 2024). Incoming shortwave radiation was partially backscattered into space by the aerosols, reducing the amount of energy incident to Earth. With a net reduction of radiative forcing, the troposphere cooled (Santer et al. 2014; Kremser et al. 2016), and a global maximum surface cooling of  $\sim 0.4$  K was achieved between June 1992 and October 1992 (Ramachandran et al. 2000). The absorption of outgoing longwave terrestrial radiation initially warmed the lower stratosphere ( $\sim 14$ – $22$  km) globally by  $\sim 1$ – $1.5$  K from September 1991 to October 1991 (Rieger et al. 2020; Ramachandran et al. 2000). However, as shown by Brown et al. (2024), the largest sulfate particles with the highest absorption efficiency of outgoing longwave radiation are measured in 1992. Hence, peak longwave radiative impacts and stratospheric temperature differences are expected in 1992.

### *b. Simulations and data preparation*

The above impacts of Mt. Pinatubo were simulated using the U.S. Department of Energy’s Earth Energy Exascale Model, version 2 (E3SMv2) (Golaz et al. 2022). These runs utilized recent

aerosol modeling capabilities, referred to as “stratospheric prognostic aerosols” (SPA) (Brown et al. 2024), which simulate sulfate aerosol formation and evolution in the stratosphere from the injection of volcanic SO<sub>2</sub> ensuring dynamical consistency between atmospheric transport and aerosol evolution. The complete implementation of E3SMv2-SPA is described by Brown et al. (2024), which details changes to the 4-mode Modal Aerosol Module microphysics (Liu et al. 2012, 2016) and validates its performance against observations.

A fully coupled simulation campaign employing E3SMv2-SPA was launched on the ne30pg2 mesh, with ~110 km horizontal resolution and 72 vertical layers up to ~0.1 hPa; the campaign is detailed by Ehrmann et al. (2024). Here we employ the ensemble of “limited variability” simulations whose climatic conditions were most similar to those which actually occurred shortly before Mt. Pinatubo’s eruption as described in Ehrmann et al. (2024). These limited variability simulations were run from June 1, 1991 to December 31, 1998 under several stratospheric SO<sub>2</sub> injections scenarios, ranging from no eruption (0 Tg SO<sub>2</sub>, the “counterfactual”) to 15 Tg SO<sub>2</sub> (~50% greater than the estimated historical eruption of ~10 Tg of stratospheric SO<sub>2</sub>). Ten ensemble members for each forcing level were generated by randomly perturbing the initial temperature field by values near machine precision. Monthly averages of field data are saved over this period. The resulting limited variability simulations are highly consistent in key quantities, especially during the first few months (Ehrmann et al. 2024).

Several steps were taken to prepare the data for the multi-step attribution process detailed in Section 3. First, all fields of interest were remapped to a 1°×1° latitude-longitude grid, and clipped between latitudes 66S–66N. This latter operation is performed to exclude missing radiation data during polar winter. Next, the time series data is trimmed from June of 1991 to May of 1993. This encompasses a two-year period over which the most significant impacts from the Mt. Pinatubo eruption occurred. Before making any further data reductions, the ensemble mean of the counterfactual simulations is computed, and this mean space-time field is subtracted from all ensemble members (including the counterfactual runs themselves). This has the effect of transforming the data from raw measurements to “impacts”; that is, the centered fields isolate the impact of Mt. Pinatubo’s eruption relative to a scenario without an eruption. We use this approach, rather than centering about a long-term climatology, as the limited variability runs are designed such that the eruption’s impact appears more clearly as a strong forcing signal. Finally, latitude-

weighted global averages are computed from the two-dimensional impact fields. This averaging results in a 24-month scalar time series for each field of interest, for each ensemble member.

### 3. Methodology

As discussed in Section 1, traditional climate attribution approaches suffer from several issues when applied to climate signals arising from forcings such as volcanic eruptions, as the characteristic time scales of the forcing effects are very short and the internal variability of the climate system may obscure climate impacts. To address these issues, we propose a novel conditional multi-step attribution method which mitigates these issues to achieve accurate attribution.

#### *a. Pathway selection*

In traditional climate fingerprinting, D&A links a climate phenomenon to a variety of possible climate forcings (e.g., natural aerosols, anthropogenic GHG emissions). This ultimately seeks a single relationship from source to impact. In contrast to this one-to-one relationship, our multi-step attribution process begins by proposing a pathway of arbitrary length and connectedness by which the climate impact may have occurred. This is generally the result of expert input based on physical understanding of the climate system (e.g., aerosols absorb longwave radiation, resulting in stratospheric warming).

In this paper, we propose three fairly simple pathways by which the eruption of Mt. Pinatubo affected the climate. The first pathway, which we refer to as the “stratosphere warming” pathway, posits that injected aerosols ( $\text{SO}_2$ , measured in teragrams mass) increase the absorption of longwave radiation at the top-of-atmosphere (FLNT, in  $\text{W/m}^2$ ), resulting in a net warming of the stratospheric temperature at the 50 hPa pressure level ( $T_{050}$ , in K). The second “surface cooling” pathway supposes that the injected aerosols reflect incoming shortwave radiation, resulting in a lower downwelling shortwave radiative flux at the Earth’s surface (FSDS, in  $\text{W/m}^2$ ), creating a net cooling effect of the temperature at a reference height of two meters (TREFHT, in K). These pathways can be treated separately, as visualized in Figures 1a and 1b, or considered as a third “combined” pathway modeling the temperature impact resulting from a single forcing, as shown in Figure 1c.



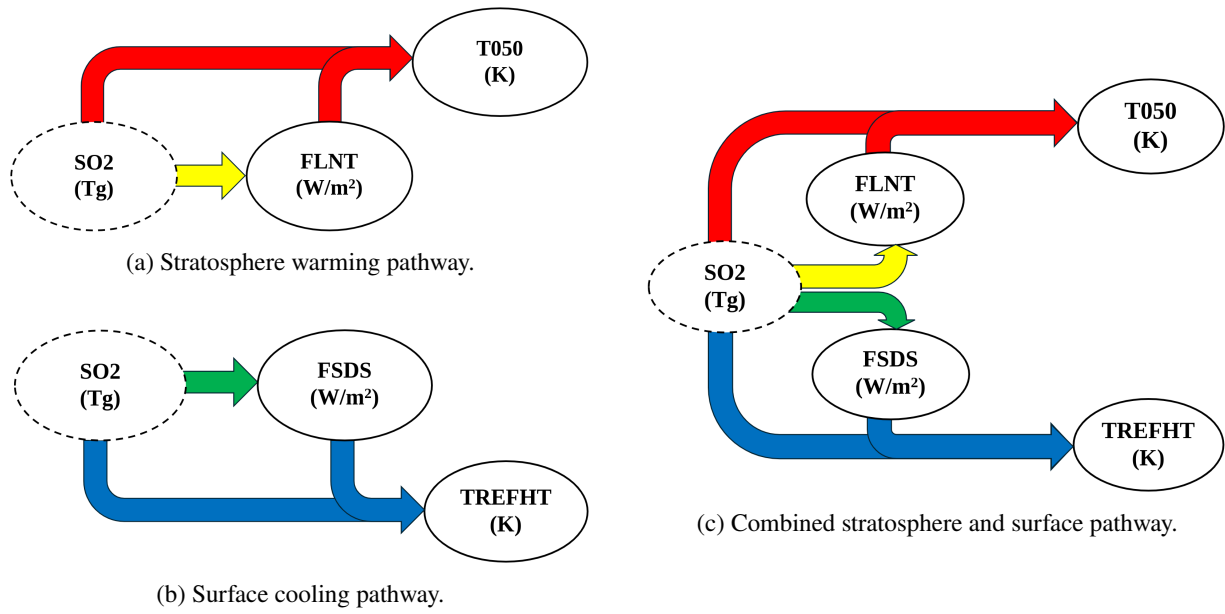


FIG. 1: Graphs representing proposed climate impact pathways, with arrows indicating a direction of influence. The source forcing ( $\text{SO}_2$ ) is marked by a dashed oval, while solid ovals indicate downstream forcing response variables. Each arrow color represents a separate regression as computed according to Section 3d.

More complex climate phenomena, such as the eruption's effect on agricultural productivity, will no doubt require commensurately more complex pathways. The following procedures can be generalized to such scenarios and will be the subject of future work. For reasons that will become apparent in Section 3e, it is important that the forcing variable (here,  $\text{SO}_2$ ) be treated as immediately upstream of every other variable, in order to capture the conditional dependence of each downstream variable on the forcing.

### *b. Peak impact analysis*

After a pathway has been proposed, average impact time series data are computed from fully-coupled climate simulations according to the process outlined in Section 2b. These simulations must necessarily include at least two different forcing magnitudes, though a greater number of simulated forcings will likely improve attribution. In this paper, we specifically include the estimated historical forcing magnitude (10 Tg  $\text{SO}_2$ ) and the counterfactual scenario (0 Tg  $\text{SO}_2$ ) along with other forcing levels. The historical forcing provides a proxy for true observational data, while the counterfactual provides a baseline against which any forcing magnitude may be compared. Here we vary the mass of  $\text{SO}_2$  injected into the stratosphere by 0, 1, 3, 5, 7, 10, 13,

and 15 Tg. Varying the forcing will be used later to approximate a functional form of the climate system with respect to the forcing magnitude. It has the added benefit of minimizing the effect of internal climate variability, which is assumed to be smaller than the effect of varying the forcing magnitude.

We first define the impact time series containing  $N_t$  time samples as  $\mathbf{q}_{v,f,e} \in \mathbb{R}^{N_t}$  for the  $v$ th variable in the pathway,  $f$ th forcing magnitude, and  $e$ th ensemble member. We emphasize that this theoretically generalizes to zonal and latitude-longitude time series data; each zonal band or coordinate (or average thereof) corresponds to a single scalar time series, and the following analysis is simply repeated for each time series in exactly the same way it would be conducted for a global average time series. In this paper, we only address global averages, and extensions to regional attribution will be the subject of future work. Examples of the global time series data can be found in Figure 4. Further, we do not consider the source forcing magnitude as a time series, but rather as a single scalar value which represents the amount of  $\text{SO}_2$  injected during June of 1991.

Note that in many cases, the characteristic time scales of a forcing’s impact on different climate fields may vary significantly. In the case of the Mt. Pinatubo eruption, a decreased surface temperature is sustained for much longer than the shortwave radiative flux decrease, as displayed in Figure 4b. This precludes any simple analysis of relationships between such variables over the entire time series (as is standard in optimal fingerprinting). As such, a carefully-designed scalar feature of the time series must be specified to more easily link variables in the proposed pathway. Here, we extract the *peak* impact from each time series. This procedure determines the maximum deviation of the impact time series from pre-forcing (i.e., pre-eruption) conditions, quantifying the effect of the forcing as a single scalar. While this somewhat limits the generalization of this approach by eliminating temporal variations in the analysis, there is practical value in understanding the maximum magnitude of a climate impact (e.g., worst case scenario for climate tipping points or best case scenario for geoengineering). We take some liberties in using the term “peak,” as this quantity may be a negative value (e.g., surface cooling is a negative temperature deviation). Depending on the desired analysis, other time-independent scalar values such as averages or integrated quantities may also serve as features.

We note that the internal variability of the climate system may introduce “spurious” peaks not directly associated with the forcing. Such spurious peaks are an inevitable feature of the chaotic

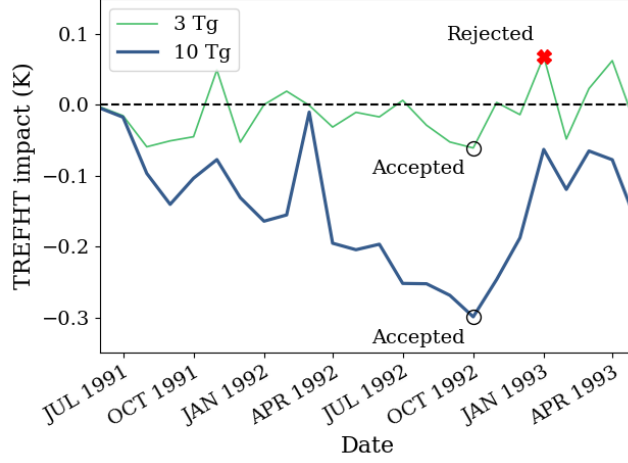


FIG. 2: Expert-informed peak finding for sample TREFHT time series data for a small 3 Tg eruption and a 10 Tg historical proxy eruption. Here, a decrease in the impact is expected, so a positive peak is rejected.

nature of the climate system, where the natural variability may obscure the forcing signal. The limited variability simulation approach detailed by Ehrmann et al. (2024) attempts to mitigate this, but is less effective over longer time horizons. In an attempt to filter some of these spurious peaks, we rely on climate expert input to reject peak impacts occurring in the direction opposite of what is expected. For example, as we expect the surface temperature to *cool* as a result of the Mt. Pinatubo eruption, we reject any spurious peaks which indicate surface *warming*. If we denote the pre-forcing state as  $q_{v,f,e}^0$ , the peak value  $k_{v,f,e}$  of time series  $q_{v,f,e}$  can be computed simply as

$$k_{v,f,e} = \begin{cases} \max(q_{v,f,e} - q_{v,f,e}^0) & \text{if increase expected,} \\ \min(q_{v,f,e} - q_{v,f,e}^0) & \text{if decrease expected.} \end{cases} \quad (1)$$

The sole exception to this peak finding procedure is, of course, the source forcing, which we have previously stated is a single scalar value indicating the forcing magnitude.

A graphical depiction of this peak finding is shown in Figure 2. The rejection of opposite-sign peaks is minimally intrusive (it does not reject same-sign spurious peaks which are not directly associated with the forcing), and is particularly useful in identifying peak impacts of low forcing magnitude ensembles for which the impact may be difficult to distinguish from internal variability. For this analysis, it is expected that the Mt. Pinatubo eruption will decrease FSDS, FLNT, and TREFHT, while increasing T050.

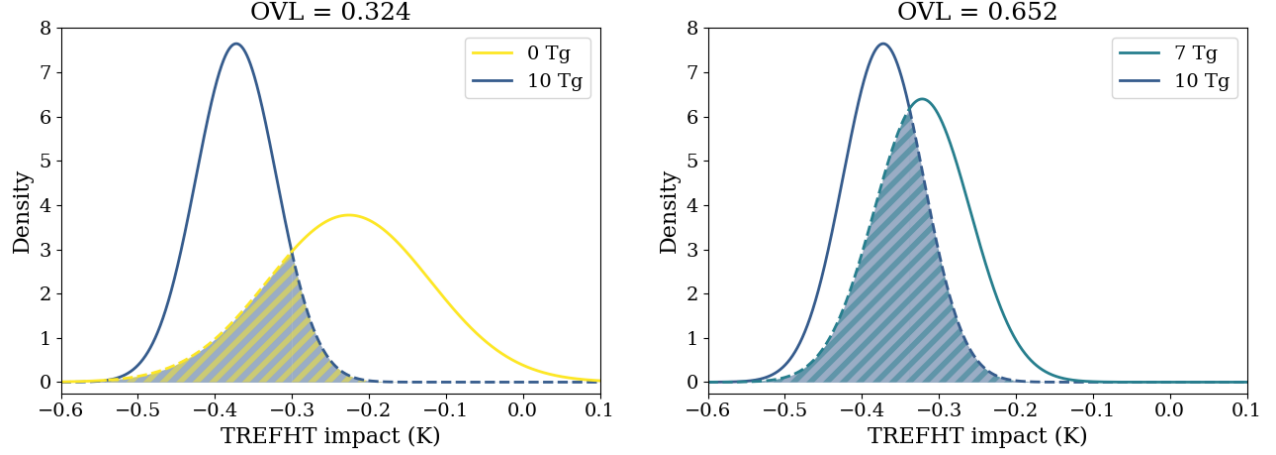


FIG. 3: Graphical depiction of overlap index between surface cooling peak impact normal distributions for 10 Tg and 0 Tg (left) and 7 Tg (right) responses. The shaded region indicates the area constituting the OVL.

### c. Overlap index

As an intermediate step not strictly required for the proposed multi-step attribution process, the peak impact data may be interrogated to understand similarities between the various forcing magnitudes. For this analysis, the peaks from all ensemble members for a given variable and forcing magnitude are collected in the vector

$$\mathbf{k}_{v,f} := [k_{v,f,1}, \dots, k_{v,f,N_e}] \in \mathbb{R}^{N_e}. \quad (2)$$

Assuming that  $k_{v,f,e} \sim P_{v,f}(\boldsymbol{\theta})$  (the peak impacts are drawn from a probability distribution  $P_{v,f}$ ), where the distribution parameters  $\boldsymbol{\theta}$  can be estimated from  $\mathbf{k}_{v,f}$ , we can approximate the probability that a measurement from one forcing magnitude ( $f_i$ ) could be misclassified as originating from a different forcing magnitude ( $f_j$ ) using a metric referred to as the “overlap index,” or OVL. Put simply, the overlap index measures the area over which two probability distributions overlap, and is graphically depicted for two normal distributions in Figure 3. This quantity can be formalized as,

$$OVL_{i,j} := \int \min(p_{v,f_i}(x), p_{v,f_j}(x)) dx, \quad (3)$$

where  $p_{v,f}(\cdot)$  is the probability density function associated with  $P_{v,f}$ . For arbitrary choices of the distribution  $P_{v,f}$ , the OVL may be computed using numerical integration. If one assumes that the

peak impacts are distributed normally, then an analytical solution exists for the OVL (Inman and Bradley 1989).

We emphasize that the OVL is not in any sense a true probability, and should not be considered an attribution tool. It is simply a measure of similarity between two distributions, and can be thought of as a *heuristic* for the probability of misclassifying the response of one forcing level to another forcing level. However, it provides insight into how different the impact response is between different forcing levels, and hints at potential difficulties in distinguishing the source of a climate impact when varied forcing levels produce similar impacts or there is a great deal of variance in peak responses. For example, the normal distributions of the 0 Tg and 10 Tg eruption TREFHT impacts (Figure 3, left) exhibit a moderate overlap of  $\sim 32\%$ , largely due to the high variability in the counterfactual response. The 7 Tg and 10 Tg responses (Figure 3, right) exhibit a high overlap of  $\sim 65\%$ , due to similarity in the mean TREFHT impacts. In both cases, this indicates that it may be difficult to distinguish between impacts resulting from these eruptions without additional information.

#### *d. Forcing response model*

With peak impacts in hand, we now seek a relationship between the peak impact of a downstream variable and any variables which are immediately upstream in the proposed pathway, as a result of varying the forcing magnitude. To begin, we introduce some notation to formalize the relationships between variables as dictated by the proposed pathway. We collect the peak impacts of a given variable from  $N_f$  forcing levels into the vector,

$$\mathbf{k}_v := [\mathbf{k}_{v,1}^\top, \dots, \mathbf{k}_{v,N_f}^\top]^\top \in \mathbb{R}^{N_e N_f}. \quad (4)$$

To separately represent the forcing magnitude, given for the  $f$ th forcing level as  $F_f$ , we create a vector with repeated instances of this scalar as  $\mathbf{f}_f := [F_f, \dots, F_f]^\top \in \mathbb{R}^{N_e}$ . Then, these are assembled for  $N_f$  forcing levels as

$$\mathbf{f} := [\mathbf{f}_1^\top, \dots, \mathbf{f}_{N_f}^\top]^\top \in \mathbb{R}^{N_e N_f}. \quad (5)$$

Pathway	FSDS	FLNT	TREFHT	T050
Stratosphere warming	$\emptyset$	SO2	$\emptyset$	SO2, FLNT
Surface cooling	SO2	$\emptyset$	SO2, FSDS	$\emptyset$
Combined	SO2	SO2	SO2, FSDS	SO2, FLNT

TABLE 1: Parent variables for proposed pathways noted in Figure 1.

Under each pathway, each variable (except for the source forcing) will have variables which are immediately upstream in the pathway. For example, under the surface cooling pathway in Figure 1b, only SO2 is immediately upstream of FSDS, while SO2 and FSDS are immediately upstream of TREFHT. We thus define a *parent set* which includes the data associated with the variables immediately upstream of a given variable, written as  $\mathcal{P}(\mathbf{k}_v)$ . Under the stratosphere warming pathway, we would thus have  $\mathcal{P}(\mathbf{k}_{FLNT}) = \{\mathbf{f}\}$ , and  $\mathcal{P}(\mathbf{k}_{T050}) = \{\mathbf{f}, \mathbf{k}_{FLNT}\}$ . The number of parents for a given variable is given as  $N_{p,v} := |\mathcal{P}(\mathbf{k}_v)|$ . The parent variable relationships for the pathways investigated in this paper are noted in Table 1.

Next, a model form must be proposed to relate downstream peak impacts as the forcing magnitude varies. While the following steps in the proposed multi-step attribution method readily generalize to more complex model forms (e.g., polynomial or logarithmic), we have found that a remarkably linear relationship exists between the peak impacts of the pathways studied in Section 4. If we concatenate the forcing magnitude and peak impacts of parent variables into the matrix  $\mathbf{K}_v := [\mathcal{P}(\mathbf{k}_v)]$ , the linear relationship in predicting downstream peak impacts can be written as,

$$\mathbf{k}_v = \mathbf{K}_v \boldsymbol{\beta}_v + \boldsymbol{\epsilon}_v, \quad (6)$$

where  $\mathbf{K}_v \in \mathbb{R}^{N_e N_f \times N_{p,v}}$ , the terms  $\boldsymbol{\beta}_v \in \mathbb{R}^{N_{p,v}}$  are the regression parameters to be estimated, and  $\boldsymbol{\epsilon}_v \in \mathbb{R}^{N_e N_f}$  are the errors for this model. For the simple pathways we propose in this paper, the first step in a pathway (e.g., predicting FSDS peak impacts from SO2 magnitude) is a univariate model. Later steps (e.g., TREFHT peak predictions from FSDS and SO2) are multivariate models. The linear model in Eq. 6 can be generalized to include an intercept term.

Under the assumption that the errors  $\boldsymbol{\epsilon}_v$  are uncorrelated, have equal variance, and are distributed normally, the maximum likelihood estimator of the model parameters  $\boldsymbol{\beta}_v$  is the ordinary least

squares estimator, given by

$$\hat{\beta}_v = [\mathbf{K}_v^\top \mathbf{K}_v]^{-1} \mathbf{K}_v^\top \mathbf{k}_v. \quad (7)$$

We take care to note that when estimating model parameters using only simulation data, it is good practice to exclude any data associated with the forcing level that will be considered the “true” forcing level for which we wish to attribute a climate response. This prevents “data leakage” where the model is trained using the “testing” dataset, unduly improving the resulting attribution purely by construction (Kapoor and Narayanan 2023). In reality, observational data would be not be excluded when training a model for deployment on unseen data, and is only excluded here for the sake of methodological evaluation.

#### *e. Bayesian attribution*

So far, with the exception of regressing against peak impacts, the proposed methodology has held similarities to traditional D&A approaches. However, it has been noted that traditional fingerprinting methods suffer from the fact that a multi-step analysis will only be at most as certain as the least certain step (Hegerl et al. 2010). To overcome this issue, we deviate in formulating a probabilistic assessment of whether a climate impact was caused by a certain climate forcing magnitude. Instead of interrogating the linear model parameters  $\hat{\beta}_v$  as in optimal fingerprinting, we frame the attribution problem from a conditional Bayesian standpoint.

Before proceeding, we again introduce useful notation. Suppose that the collection of climate simulations has been computed across a discrete set of forcing magnitudes  $\mathcal{F}$ , where  $N_f := |\mathcal{F}|$ . The unknown forcing random variable is denoted by  $F$ . Further, suppose that some “observational” peak impact dataset is available for all downstream climate variables, and we know the forcing magnitude associated with these observations. This can be considered a single measurement of the “true” forcing level for which we will assess correct attribution of the proposed method. This set of observed data for  $N_v$  variables (*excluding the forcing magnitude*), can be denoted as  $\mathcal{O} := \{k_1^O, \dots, k_{N_v}^O\}$ . The forcing magnitude is not included as it is not treated as an observed quantity. In this paper, the radiative flux variables (FSDS and FLNT) and temperature variables (TREFHT and T050) are thus treated as observed variables.

Following the above notation, the associated Bayes’ rule for attributing a particular forcing level  $f$  can be written as,

$$\text{posterior}(F = f|\mathcal{O}) = \frac{\text{likelihood}(\mathcal{O}|F = f)\text{prior}(f)}{\sum_{f' \in \mathcal{F}} \text{likelihood}(\mathcal{O}|F = f')\text{prior}(f')}. \quad (8)$$

In layman’s terms, Eq. 8 computes the (posterior) probability that a forcing level  $f$  did indeed occur, conditioned on observational data of the true forcing level. The likelihood terms are computed from our models of the forcing response, i.e., our prediction of the climate response given a certain forcing level. This encodes our modeling uncertainty: the lower the error in the prediction of each observed response in each step of the proposed pathway, the higher the likelihood, and the higher the posterior. Of particular importance is the potential for multi-step pathways to improve this inference, as computing the likelihoods with *more* observational information stands to decrease uncertainty. Such a conditional approach differs significantly from statistically-independent approaches (Hegerl et al. 2010), and as will be shown shortly, improves the ability to successfully attribute a climate response to the correct forcing level. Computing the likelihood terms is somewhat involved; details and a worked example are given in the appendix.

The prior terms encode our belief that a certain forcing level has, in truth, occurred. While more general prior distributions are likely achievable, in this work we will choose two user-defined prior distributions signifying different levels of knowledge of a volcanic eruption, and will investigate the sensitivity of the posteriors to these choices.

In this work, the “observational” dataset is not derived from historical measurements. Instead, a single simulated forcing level is treated as the observational dataset, and the scalar measurement for each variable is computed as the ensemble mean of the peak impacts. That is, for the “observational” forcing level  $f_O$ ,

$$k_v^O = \frac{1}{N_e} \sum_{e=1}^{N_e} k_{v,f_O,e}. \quad (9)$$

This “true” forcing level is the same set which is deliberately excluded from estimating the forced model response for the sake of preventing data leakage and assessing the robustness of this multi-step attribution procedure, as noted in Section 3d.

Once posterior probabilities have been computed for every available simulated forcing level, they may be compared to each other and a relative assessment of attribution made. Establishing a



firm threshold (e.g., a posterior greater than 0.9) for attribution is somewhat arbitrary and open to debate. Although frameworks exist for supporting certain conclusions (such as Bayes factors), in this manuscript we will simply present the computed posterior probabilities and largely leave out statements of absolute attribution unless they are overwhelmingly obvious.

#### 4. Results

We now turn to applying the methodology described above to the 1991 eruption of Mt. Pinatubo and the purported resulting stratosphere warming and surface cooling, following the pathways established in Section 3a. To motivate the use of intermediate physical effects (i.e., FSDS and FLNT) in such multi-step pathways, throughout this section we will make comparisons against the related single-step pathway; that is, relating a temperature impact directly from the  $\text{SO}_2$  forcing magnitude. Similarly, we will show that the pathway combining the surface cooling and stratosphere warming effects improves attribution strength beyond that of its separate component pathways. Such multi-step approaches demonstrate that the proposed attribution framework benefits from additional information, while traditional D&A methods are typically limited by the single weakest step in the analysis.

According to the strategy outline in Section 2b, we simulate the eruption and the following two years under  $N_f = 8$  different forcing scenarios, each characterized by the mass of  $\text{SO}_2$  injected into the stratosphere by the eruption: 0 (no eruption, counterfactual), 1, 3, 5, 7, 10 (“observational” forcing level), 13, and 15 Tg  $\text{SO}_2$ . We compute  $N_e = 10$  ensemble members for each forcing level, for a total of 80 runs. Latitude-weighted global averages of the pathway variables are computed, and the ensemble means are displayed in Figure 4. Note that while the T050 signal is fairly clear and easy to distinguish between the different forcing levels, the FLNT, FSDS, TREFHT signals are much noisier in comparison. In particular, the expert-informed peak filtering procedure stated in Eq. 1 rejects several spurious *positive* TREFHT deviations which are observed for low-mass simulations (1, 3, and 5 Tg) nearly two years after the eruption. These are clearly not directly associated with the eruption, and rejecting them helps to delineate the volcanic impacts. By similarly applying the expert-informed peak filtering to the counterfactual runs, we are instantiating the same bias in natural variability alone. Note that the FLNT plot shows two negative peaks: the first occurs around September 1991 when the total mass of  $\text{SO}_2$  first becomes zonally distributed while precipitation

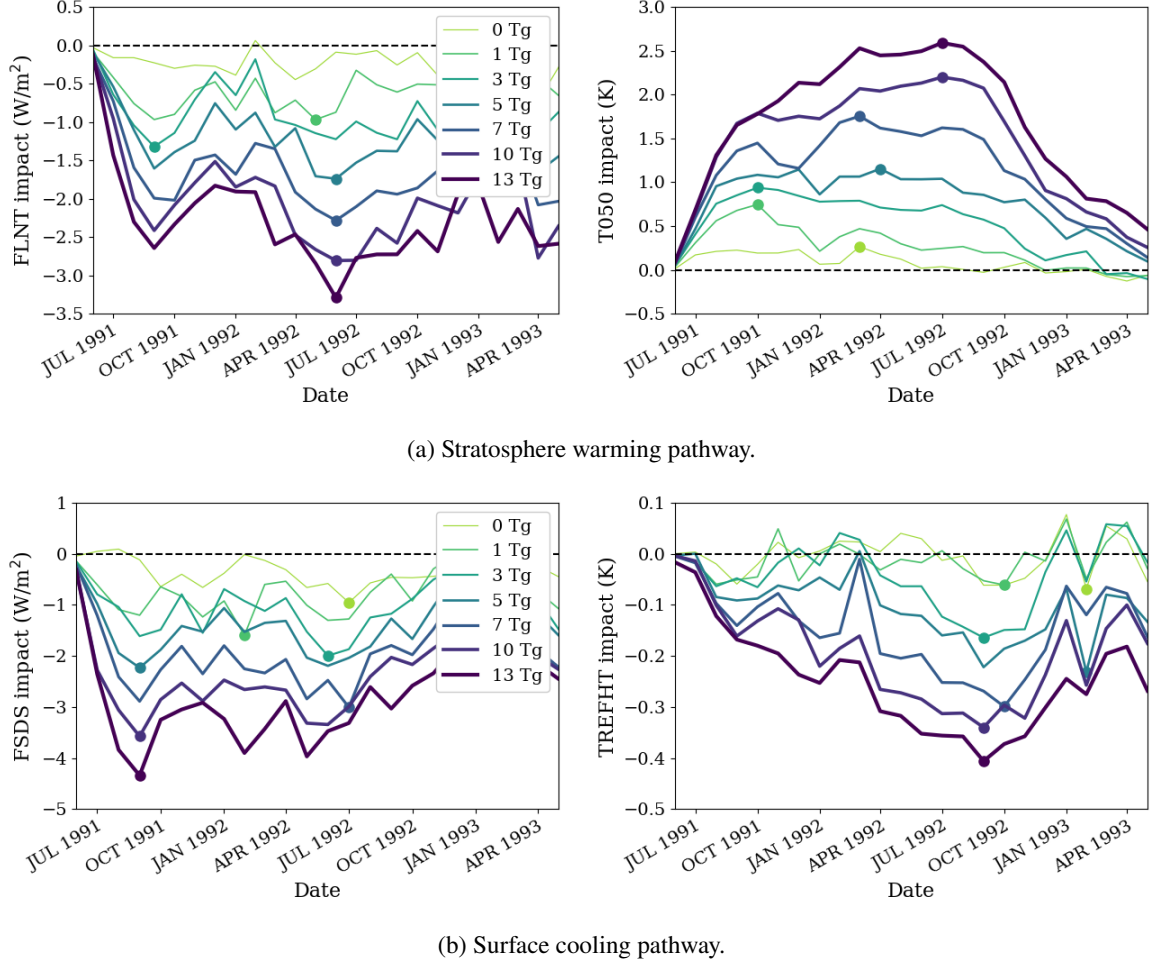


FIG. 4: Latitude-weighted global average ensemble mean impact for variables in proposed pathways under various forcing magnitudes. Peak ensemble mean impacts are marked with a dot, and the zero impact line is marked with a dashed black line.

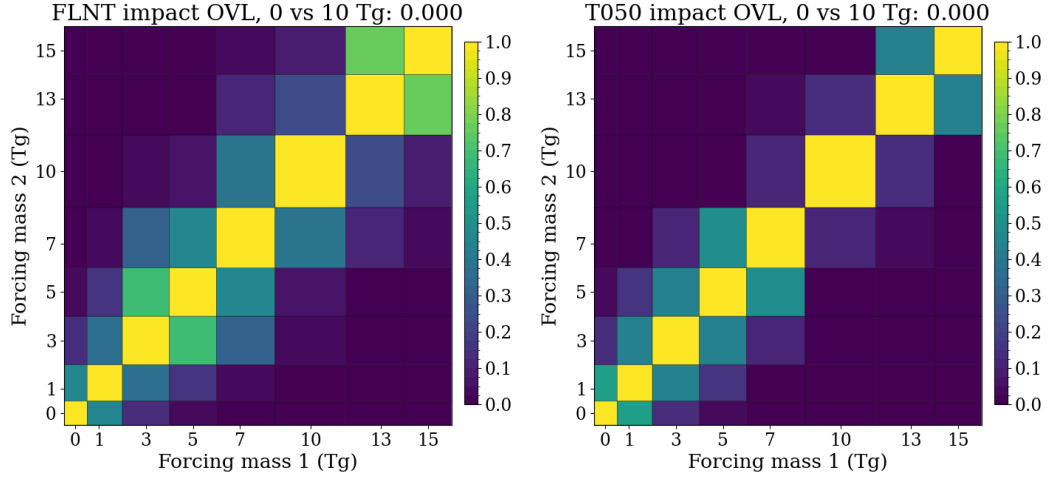
out of the atmosphere is still low, and the second peak occurs in 1992 when the particle sizes grow largest, as mentioned previously (Brown et al. 2024).

To better understand the similarity in peak impact responses for the pathway variables, we can examine the overlap indices for distributions fitted to the computed peak impact data. Here, we make the generous assumption that the peak impacts for each forcing level are distributed normally. Ten samples is a rather small population size, but we make this assumption for the sake of simplicity. With larger ensembles, non-parametric distributions may provide more detailed measurements. Figure 5 displays the pairwise OVL values for all forcing levels, for each pathway variable. The diagonal elements are exactly unity, as identical density functions overlap entirely. In general, the stratosphere warming pathway variables exhibit higher dissimilarity in the forcing

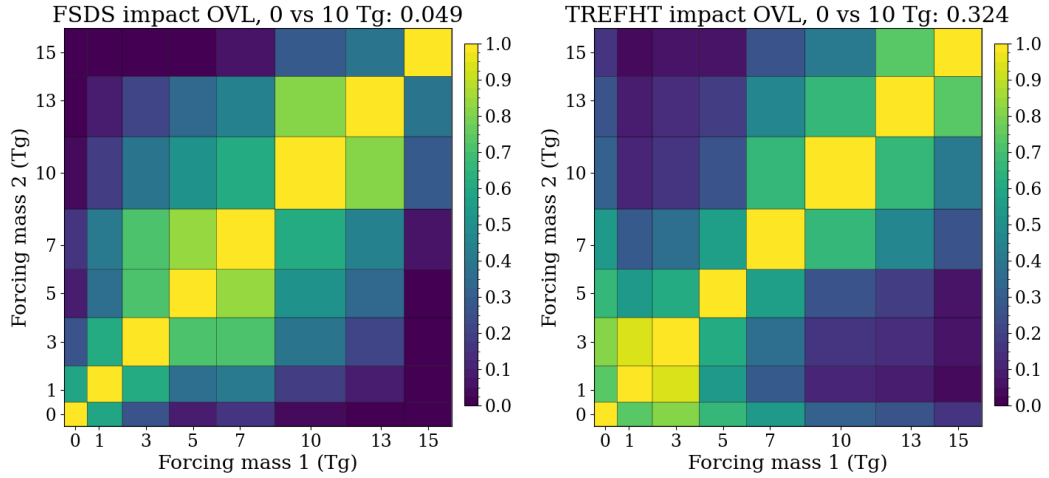
response distributions, with low OVL values except for forcing levels which differ by 2-3 Tg. This is particularly true for the T050 response, for which the 10 Tg response share little similarity with any other forcing level. The surface cooling variables (FSDS and TREFHT) are quite the opposite, indicating high overlap between forcing levels even between those which differ by 4-6 Tg. Of particular note is the fact that the counterfactual and 10 Tg TREFHT responses exhibit an overlap of  $\sim 32\%$ . This gives a *rough* estimate that the chance of misclassifying a 10 Tg response as a counterfactual response (or vice versa) is nearly one in three. In fact, all forcing magnitudes below 10 Tg exhibit an OVL with the counterfactual distribution greater than 50%. Seemingly, distinguishing a large volcanic eruption response from a non-eruption response, solely by surface temperature measurements, is quite difficult. This is due to the very high noise level associated with the TREFHT signal, and hints at possible challenges in successfully identifying the correct Pinatubo forcing level. Relying on a single variable for the identification thus appears extremely challenging, and so we turn to incorporating the above proposed multi-step pathways.

Linear models for each step in the proposed pathway are computed according to Eq. 7. As mentioned in Section 3d, we deliberately remove any 10 Tg simulation data from this calculation, as this represents the “true” data whose response we wish to attribute. The resulting global average peak impact fits are plotted in Figure 6, including the 10 Tg peak values for the sake of completeness. We observe extremely strong linear relationships between the stratosphere warming variables, indicated by an  $R^2$  greater than 0.9 in predicting the FLNT and T050 response. While not as pronounced, the prediction of FSDS from forcing magnitude (Figure 6b) is still quite robust, with an  $R^2$  value of  $\sim 0.77$ . This lends some credence to the use of peak impacts in our model: while the time-varying relationships between forcing level, radiative fluxes, and temperature are clearly highly non-linear from Figure 4, there exists a plausible linear relationship in peak impact space. There is not quite as strong a relationship in predicting TREFHT from SO<sub>2</sub> and FSDS, however, indicated by an  $R^2$  value of approximately 0.62. This is no doubt a function of the climate system’s internal variability and comparatively noisy TREFHT signal. Linear models for the single-step pathways (predicting temperature impacts directly from forcing magnitude) are included in the supplementary material.

Using the linear fits computed for each step in the proposed pathway, we now compute the posterior probabilities that each forcing level (0 to 15 Tg stratospheric SO<sub>2</sub>) might result in the



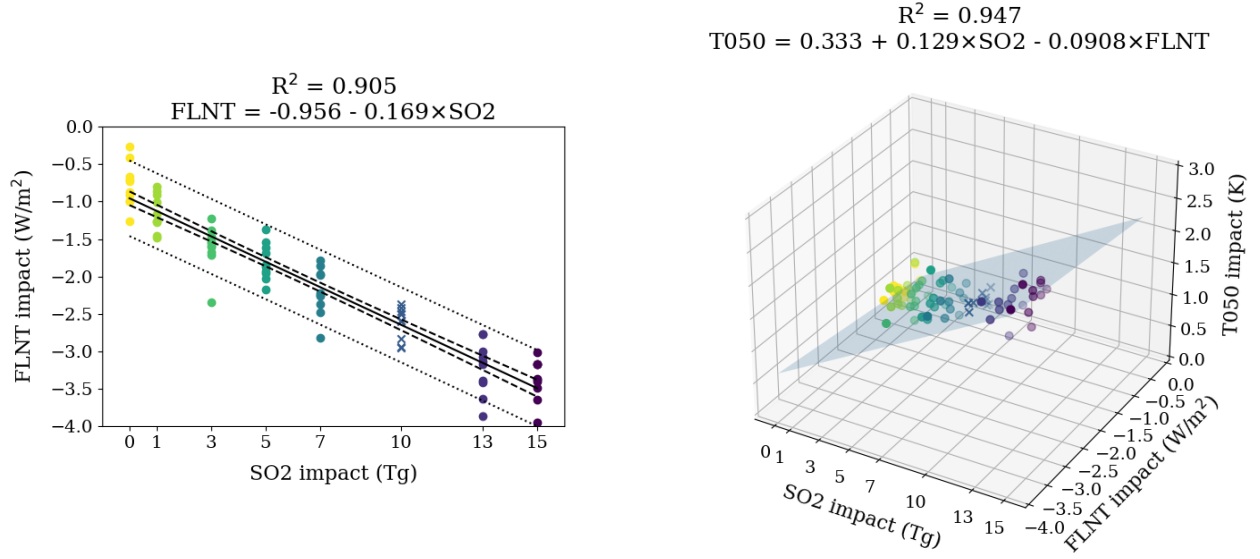
(a) Stratosphere warming pathway.



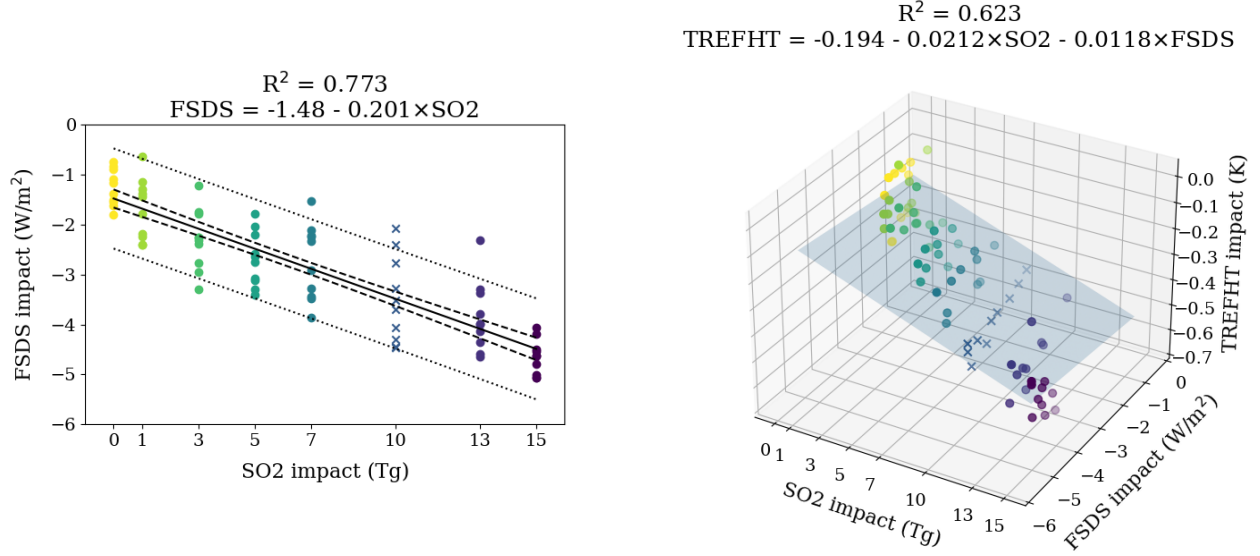
(b) Surface cooling pathway.

FIG. 5: Overlap indices between pairs of forcing level global average peak impact responses. Each rectangle is scaled according to the forcing level granularity. The OVL between the 0 Tg counterfactual and 10 Tg historical proxy is noted in the figure titles.

“observed” response, as represented by the ensemble mean of the 10 Tg forcing peak impact data. To begin, we must define prior probabilities associated with each forcing level. We use prior distributions specified two ways: a “well specified” prior and a “poorly specified” prior. These priors represent situations in which it is known that a volcano erupted and a rough estimate of the forcing mass can be made, but there is uncertainty in this mass estimate. This places equal, large prior probabilities on several forcing masses, and all remaining forcing levels are assigned a low prior probability. The well specified prior includes a large probability on the “observed” 10 Tg



(a) stratosphere warming pathway



(b) Surface cooling pathway

FIG. 6: Global average impact linear regression fits for surface cooling pathway. Univariate model plots (left) include the OLS fit (solid line), 90% confidence interval (dashed line), and 90% prediction interval (dotted line). Multivariate model plots (right) display the best fit plane (shaded gray). Linear model parameters and  $R^2$  values are noted in the figure titles. The 10 Tg data are not included in computing the regression, and are marked separately on the plots.

forcing, while the poorly specified prior does not. These two prior sets help demonstrate the risk of misspecifying the prior, to which we will show our multi-step attribution method is fairly robust. The prior values are noted in Table 2.

Prior set	0 Tg	1 Tg	3 Tg	5 Tg	7 Tg	10 Tg	13 Tg	15 Tg
Well specified	0.02	0.02	0.02	0.02	0.30	0.30	0.30	0.02
Poorly specified	0.02	0.02	0.30	0.30	0.30	0.02	0.02	0.02

TABLE 2: Prior probabilities for simulated forcing levels.

Included in the supplementary material are attribution results under a “volcanic agnostic” prior distribution, which represents a scenario in which it is *not* known that a volcano erupted. This relies on a general understanding that volcanic eruptions are rare and assigns almost all prior probability to the counterfactual (0 Tg) case, with equal, small values for all volcanic forcings. While somewhat contrived (a volcanic eruption cannot realistically occur without being noticed), this relates to geoengineering attribution more broadly, where the impact of independent actors may not be readily apparent.

Under these prior sets, the global average impact posteriors for each forcing level are shown in Figs. 7 and 8. These include results for the stratosphere warming pathway (whose graph is depicted in Figure 1a), surface warming pathway (Figure 1b), and combined pathway (Figure 1c), both for multi-step pathways and corresponding single-step pathways (relating forcing and temperature response directly). The posteriors are marked in blue and the prior distribution is displayed in orange, in order to visualize the influence of the prior.

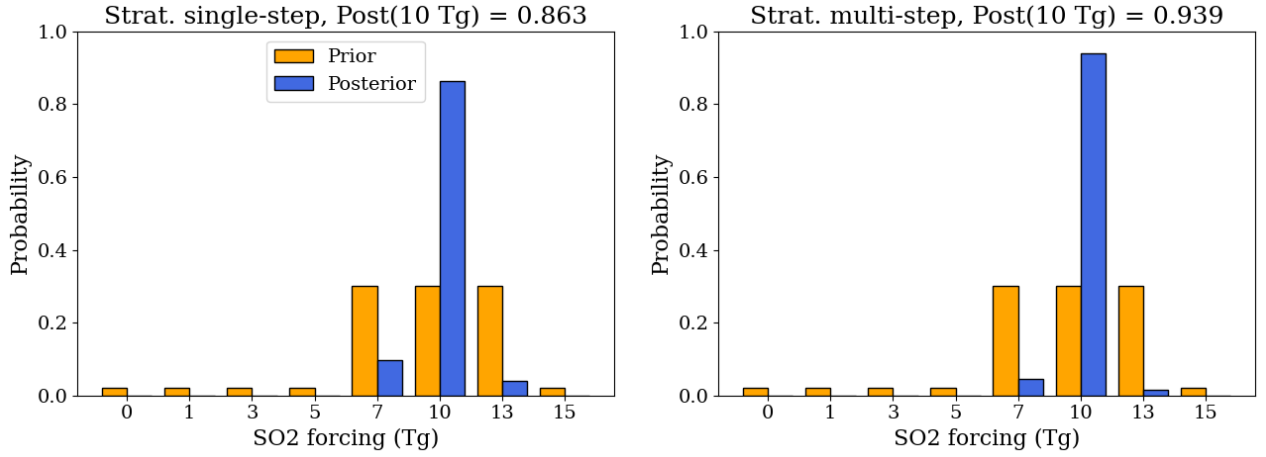
We first address the posteriors computed under the well specified prior set, shown in Figure 7. It is immediately clear that the stratosphere warming pathway has little difficulty in correctly identifying the 10 Tg forcing as the most likely scenario. Even the single-step pathway, attributing the forcing magnitude solely from temperature measurements, achieves a very high posterior of  $\sim 86\%$ . The addition of FLNT as an intermediate variable improves this assessment by approximately 8%. The surface cooling pathway, on the other hand, provides a more significant attribution challenge, with the single-step pathway differing very little from the prior distribution. This indicates that the linear model predicting TREFHT from SO<sub>2</sub> provides little useful information to help distinguish the 10 Tg forcing response. However, the addition of FSDS in the multi-step pathway enables a slightly stronger attribution statement, increasing the 10 Tg posterior probability to  $\sim 53\%$ . When these separate pathways are combined, the resulting accurate attribution is obviously dominated by the low uncertainty in the stratosphere warming models. While the improvement from adding the single-step surface cooling pathway to the single-step stratosphere pathway is minimal, the effect

of adding the multi-step surface cooling pathway to the multi-step stratosphere warming pathway improves the posterior probability for the 10 Tg forcing from 94% to 97%, effectively halving the 10 Tg attribution uncertainty (6% to 3%). This demonstrates that our approach benefits from incorporating multiple downstream effects and is not simply dictated by the strongest individual signal.

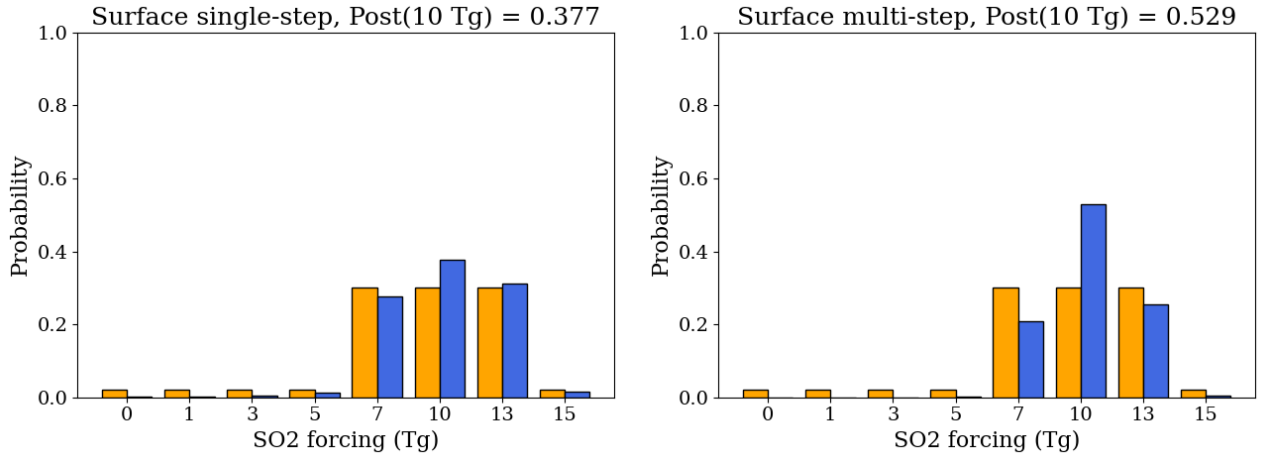
Next, we investigate attribution results under poorly specified priors, displayed in Figure 8. In almost all cases, including the multi-step stratosphere warming pathway, the proposed method either incorrectly identifies the 7 Tg forcing as the most likely forcing magnitude, or the posteriors for the 7 and 10 Tg forcing levels are very similar. In the latter case, even if the 10 Tg forcing magnitude is most likely, the uncertainty associated with this assessment precludes any absolute attribution statement. This is the direct result of specifying a relatively large prior probability on the 7 Tg forcing, weighting the 7 Tg likelihood even when the 10 Tg likelihood is greater. However, under the combined multi-step pathway, despite the incredibly small prior assigned to the 10 Tg forcing, the method is able to correctly identify the 10 Tg as most likely, with a posterior probability three times larger than that of the 7 Tg forcing. In this case, a fairly strong relative attribution statement can be made. Again, this result reveals that incorporating additional forcing response information improves the robustness of the proposed attribution method. This contrasts strongly with traditional attribution methods, which generally do not improve with the inclusion of additional climate variables or steps in the climate model.

## **5. Discussion**

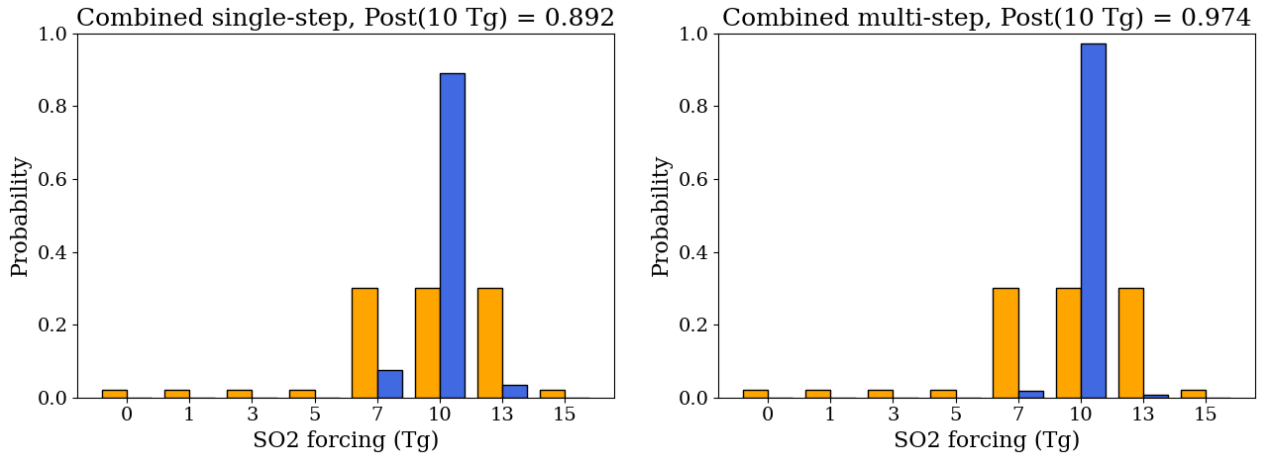
In this paper we have developed a novel multi-step approach to climate impact attribution, demonstrated for a short-term point-source forcing as characterized by the 1991 eruption of Mt. Pinatubo, but potentially more broadly applicable to other forcings. This method leverages strong relationships in the peak impacts of variables related to the eruption's effects on the climate, building a conditionally-dependent “pathway” along which a downstream effect is linked to the source forcing. A Bayesian formulation allows for rigorous quantification of uncertainty in attributing such effects to specific forcing levels, supplying a new tool for analysts to better understand the sensitivity of the climate to varying forcings. A multi-step approach was demonstrated for the stratosphere warming and surface cooling effects of the Mt. Pinatubo eruption, exhibiting clear attribution



(a) Stratosphere warming pathway.



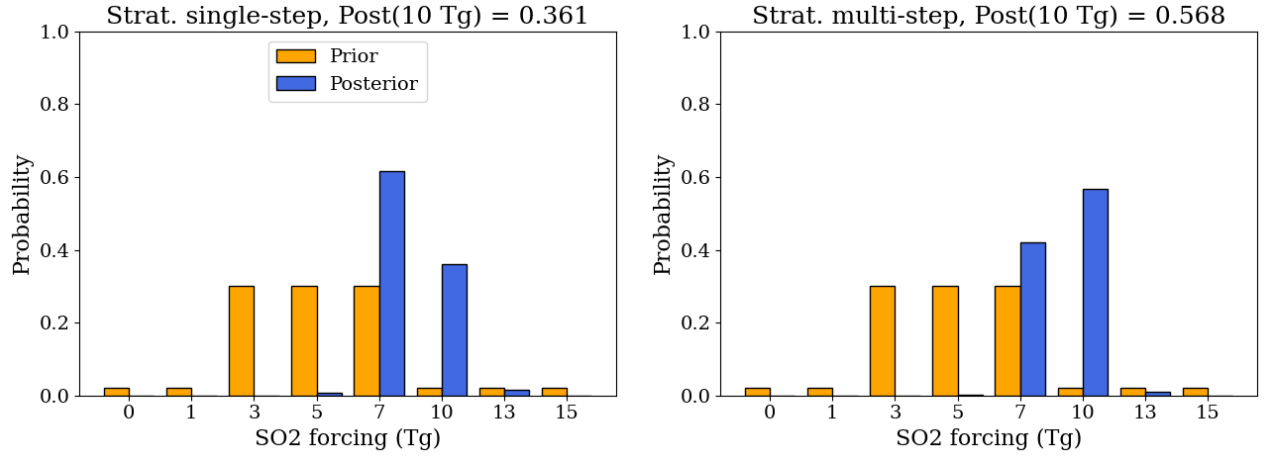
(b) Surface cooling pathway.



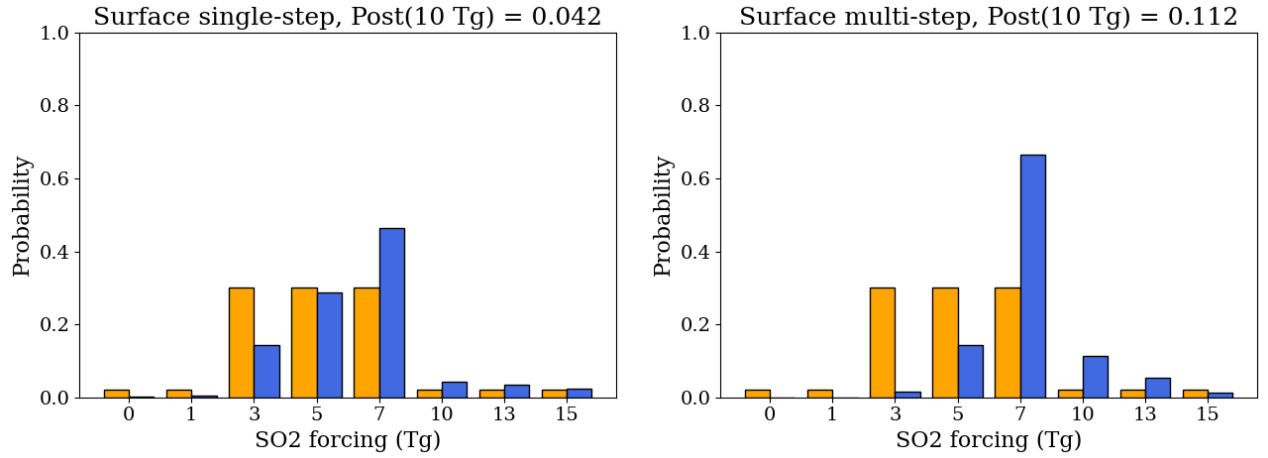
(c) Combined pathway.

FIG. 7: Posterior probabilities (blue) under well specified prior distribution (orange), for stratosphere warming only (top), surface cooling only (middle) and combined pathways (bottom), for single-step (left) and multi-step (right) pathways. The 10 Tg posterior is noted in the figure titles.

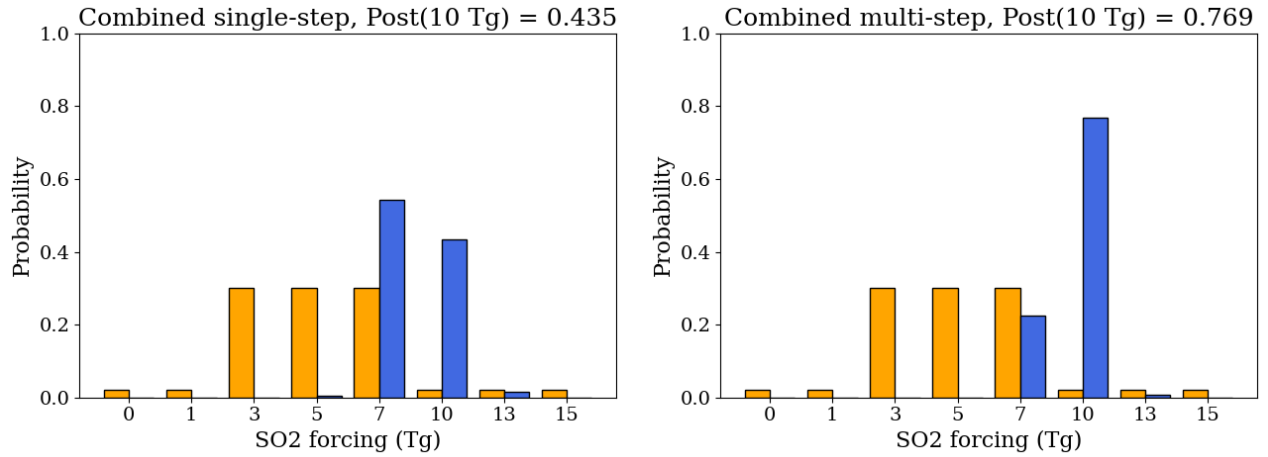




(a) Stratosphere warming pathway.



(b) Surface cooling pathway.



(c) Combined pathway.

FIG. 8: Posterior probabilities (blue) under poorly specified prior distribution (orange), for stratosphere warming only (top), surface cooling only (middle) and combined pathways (bottom), for single-step (left) and multi-step (right) pathways. The 10 Tg posterior is noted in the figure titles.

of the true forcing level and robustness to user-defined priors. The use of intermediate climate variables including the top-of-atmosphere longwave radiation flux and surface shortwave radiation flux, as well as modeling multiple forcing effects in a single pathway, greatly improves attribution and demonstrates the benefit of expert understanding of the climate system. In comparison, single-step pathways from source to effect produce less certain attribution in the best case, and incorrect attribution in the worst case. For future applications, the method is readily generalizable to regional attribution studies, more complex pathways, alternative data features besides peak impacts, more detailed impact response models, and more informative prior distributions. Despite the observed success for this particular problem, several questions remain regarding potential modeling improvements and broader utility for other climate forcing events.

First, the method relies heavily on user input beyond proposing a pathway. Selecting the number and granularity of forcing levels has so far been a somewhat arbitrary decision, and we do not offer strict guidelines on how to perform this selection beyond suggesting that the range include the “true” forcing level and the counterfactual. Further, assigning a specific threshold above which a posterior probability accomplishes “attribution” is similarly arbitrary, and the user must instead rely on relative attribution. Second, it remains to be seen whether this methodology can succeed for more complex pathways. Linking climate forcings to human-relevant impacts (such as agricultural productivity) will necessitate more complex pathways with potentially disjoint steps. Strong linear relationships in peak impact space may not exist for effects far downstream of the source forcing, and higher variance may contribute significantly to increased uncertainty. Finally, the method may require significant modification to extend to practical short-term forcing such as geoengineering or climate tipping points. Such events are often characterized by sustained forcings from multiple spatial locations, and the use of peak impacts in building the linear models may not be applicable. Designing features to characterize such forcings requires careful consideration of their physical mechanisms.

Despite the above questions, this novel approach offers a fresh perspective on climate attribution, enabling a true multi-step procedure which is not limited by the strictures inherent in traditional optimal fingerprinting methodologies. In concrete terms, climate engineering through stratospheric aerosol injection highlights a potential application of this work. The ARISE-SAI simulation campaign (Richter et al. 2022) indicates that by 2067, 10 Tg of injected  $\text{SO}_2$  per year will be

necessary to limit the surface temperature rise to 1.5° C. In practice, it may be extremely difficult for the global community to quantitatively assess the effectiveness of these interventions in the face of natural variability, leading to potential perceived failures of this engineering strategy (Keys et al. 2022). New attribution formalisms, like that presented here, have the potential to incorporate mechanistic knowledge as additional conditional information to increase the confidence that the strategies are or are not working. While the methods and results discussed here are simplified for the sake of clarity, this opens the door to a host of interesting analyses and equips climate scientists with a new rigorous, probabilistic framework for tackling attribution for a multitude of modern climate problems.

*Acknowledgments.* We thank the members of the CLDERA LDRD team for helpful discussions. In particular, we thank Benjamin Wagman for assistance in characterizing the high-altitude temperature response, Meredith Brown and Justin Li for initial work on fingerprinting and variability, Joseph Hart, Mamikon Gulian, Indu Manickam, J. Jake Nichol, Irina Tezaur, Kara Peterson, and Lyndsay Shand for helpful discussions.

Sandia National Laboratories is a multimission laboratory managed and operated by National Technology & Engineering Solutions of Sandia, LLC, a wholly owned subsidiary of Honeywell International Inc., for the U.S. Department of Energy’s National Nuclear Security Administration under contract DE-NA0003525. This work was funded through Sandia’s Laboratory Directed Research and Development program. The views expressed in the article do not necessarily represent the views of the U.S. Department of Energy or the United States Government.

This research used resources of the National Energy Research Scientific Computing Center (NERSC), a Department of Energy Office of Science User Facility using NERSC award BER-ERCAP0026535.

This article has been authored by employees of National Technology & Engineering Solutions of Sandia, LLC under contract DE-NA0003525 with the U.S. Department of Energy (DOE). The employees own all right, title and interest in and to the article and is solely responsible for its contents. The United States Government retains and the publisher, by accepting the article for publication, acknowledges that the United States Government retains a non-exclusive, paid-up, irrevocable, world-wide license to publish or reproduce the published form of this article or allow others to do so, for United States Government purposes. The DOE will provide public access to these results of federally sponsored research in accordance with the DOE Public Access Plan.

## APPENDIX

### **Multi-step bayesian attribution**

For the sake of brevity, the calculation of posterior probabilities appears somewhat opaque in Section 3e. Here, we explain the computations in more detail and include a worked example for the proposed surface cooling pathway.

### a. Derivation

As noted in Section 3e, the posterior probability for the  $f$ th forcing level conditioned on the observed response of all downstream variables is given by,

$$\text{posterior}(F = f | \mathcal{O}) = \frac{\text{likelihood}(\mathcal{O} | F = f) \text{prior}(f)}{\sum_{f' \in \mathcal{F}} \text{likelihood}(\mathcal{O} | F = f') \text{prior}(f')}. \quad (\text{A1})$$

Recall that the observational dataset  $\mathcal{O} := \{k_1^O, \dots, k_{N_v}^O\}$ , where the individual observations are the ensemble means of the peak impacts for each variable, is selected from a particular “true” forcing level (in this paper, 10 Tg SO<sub>2</sub>), as defined in Eq. 9. The source forcing magnitude is not a member of the observational dataset, and the priors are treated as given.

Next, we define the forcing level random variable  $F$  and a random variable for the observational peak impact data point for each variable as  $K_v$ . Using the shorthand  $\mathcal{L}_f$  to denote the likelihood for the  $f$ th forcing level, we can formalize the likelihood as a function of the  $N_v$  downstream variables (all variables excluding the forcing magnitude) in a proposed pathway as

$$\mathcal{L}_f := \text{likelihood}(\mathcal{O} | F = f), \quad (\text{A2})$$

$$= p(K_1 = k_1^O, \dots, K_{N_v} = k_{N_v}^O \mid F = f), \quad (\text{A3})$$

$$= p(K_1 = k_1^O \mid F = f) \prod_{v=2}^{N_v} p(K_v = k_v^O \mid F = f, K_1 = k_1^O, \dots, K_{v-1} = k_{v-1}^O), \quad (\text{A4})$$

as a result of the chain rule of probability. If  $N_v = 1$ , the product term in Eq. A4 is neglected.

Recall the parent set  $\mathcal{P}(\cdot)$ ; if a variable is not a parent of a given variable, then it does not influence the associated likelihood term. Thus, Eq. A4 can be written concisely as

$$\mathcal{L}_f = \prod_{v=1}^{N_v} p(K_v = k_v^O \mid F = f, \mathcal{P}(K_v) = \mathcal{P}(k_v^O)), \quad (\text{A5})$$

where we slightly abuse the parent set notation. In the event that the forcing magnitude is a parent variable, the implied repetition of  $F = f$  is redundant.

Recall that we have computed linear models for each downstream variable with regression parameters given by Eq. 7. Under the assumption that the errors are distributed normally, the

conditional peak impact predictions are distributed such that

$$K_v \mid F, \mathcal{P}(K_v) = \mathcal{P}(k_v^O) \sim \mathcal{N}\left(\left(\widehat{\beta}_{F \rightarrow v} F + \sum_{j \in \mathcal{P}(K_v)} \widehat{\beta}_{j \rightarrow v} K_j\right), \widehat{\sigma}_v^2\right), \quad (\text{A6})$$

where we again abuse notation in writing the  $\widehat{\beta}_{j \rightarrow v}$  as the linear regression parameter associated with predicting the  $v$ th variable as a function of the variable whose *name* is  $j$ , as indexed by the parent variable set. The term  $\widehat{\sigma}_v^2$  is the sample variance of the residuals of the linear model which predicts the  $v$ th variable. Under this distribution, the likelihood terms may be analytically computed as

$$p\left(K_v = k_v^O \mid F = f, \mathcal{P}(K_v) = \mathcal{P}(k_v^O)\right) = \frac{1}{\sqrt{2\pi\widehat{\sigma}_v^2}} \exp\left(-\frac{1}{2\widehat{\sigma}_v^2} \left(k_v^O - \left(\widehat{\beta}_{F \rightarrow v} f + \sum_{j \in \mathcal{P}(K_v)} \widehat{\beta}_{j \rightarrow v} k_j^O\right)\right)^2\right). \quad (\text{A7})$$

Equation A7 is plugged into Eq. A4, which in turn is substituted into Eq. A1 for each  $f$ th forcing level, arriving at the posterior probability for a given forcing level conditioned on the “true,” observed downstream variables.

### *b. Worked example*

The multitude of indices in Eqs. A1-A7 is admittedly confusing. Here, we step through a worked example using the surface cooling pathway visualized in Figure 1b. We begin by assuming that the 10 Tg forcing level is the “observed” response, and set  $f_O = 10$ . Say we would like to calculate the probability of misattributing the observed response to a 7 Tg forcing level; we thus set  $f = 7$ . For the sake of clarity, we replace the variable indices  $v$  with the names of the relevant variables, shortened to “S” for SO<sub>2</sub>, “R” for FSDS, and “T” for TREFHT. Thus, the FSDS and TREFHT observations are computed as

$$k_R^O = \frac{1}{N_e} \sum_{e=1}^{N_e} k_{R,10,e}, \quad (\text{A8})$$

$$k_T^O = \frac{1}{N_e} \sum_{e=1}^{N_e} k_{T,10,e}. \quad (\text{A9})$$

Variable	$k_v^O$	$\hat{\beta}_0$	$\hat{\beta}_{\text{SO2} \rightarrow v}$	$\hat{\beta}_{\text{FSDS} \rightarrow v}$	$\hat{\sigma}_v^2$
FSDS	-3.50233	-1.47859	-0.20066	N/A	0.34948
TREFHT	-0.37228	-0.19407	-0.02122	-0.01180	0.00650

TABLE A1: Observed values and regression parameters for variables in the surface cooling pathway. An intercept term  $\hat{\beta}_0$  is included in the regression.

Given linear regression parameters  $\hat{\beta}_R$  and  $\hat{\beta}_T$ , the likelihood terms can be computed as

$$p(K_R = k_R^O \mid F = 7) = \frac{1}{\sqrt{2\pi\hat{\sigma}_R^2}} \exp\left(-\frac{1}{2\hat{\sigma}_R^2} (k_R^O - \hat{\beta}_{S \rightarrow R} \cdot 7)^2\right), \quad (\text{A10})$$

$$p(K_T = k_T^O \mid F = 7, K_R = k_R^O) = \frac{1}{\sqrt{2\pi\hat{\sigma}_T^2}} \exp\left(-\frac{1}{2\hat{\sigma}_T^2} (k_T^O - \hat{\beta}_{S \rightarrow T} \cdot 7 - \hat{\beta}_{R \rightarrow T} \cdot k_R^O)^2\right). \quad (\text{A11})$$

The above process is repeated for every forcing level in the forcing set  $\mathcal{F}$  in order to compute the evidence, or the denominator of Eq. A1. Finally, the posterior probability that a 7 Tg forcing occurred is computed as

$$p(F = 7 \mid K_R = k_R^O, K_T = k_T^O) = \frac{p(K_R = k_R^O \mid F = 7) p(K_T = k_T^O \mid F = 7, K_R = k_R^O) \text{prior}(7)}{\sum_{f' \in \mathcal{F}} p(K_R = k_R^O \mid F = f') p(K_T = k_T^O \mid F = f', K_R = k_R^O) \text{prior}(f')}. \quad (\text{A12})$$

To work through the posterior calculations for the multi-step surface cooling pathway, we provide values for the regression parameters and the “observed” peak impacts for each variable in Table A1. The regression parameters were previously displayed in Figure 6b. The well specified priors from Table 2 are used. The resulting likelihood and posterior values, computed entirely from the forcing levels, observed peak impacts, and regression parameters, are given in Table A2. These posterior values match those displayed in the right figure of Figure 7b.

	$f = 0$	$f = 1$	$f = 3$	$f = 5$	$f = 7$	$f = 10$	$f = 13$	$f = 15$
$p(K_R = k_R^O \mid F = f)$	0.00193	0.00581	0.03743	0.15214	0.39000	0.67456	0.41365	0.16782
$p(K_T = k_T^O \mid F = f, K_R = k_R^O)$	0.12130	0.23996	0.76278	1.83793	3.35679	4.92820	3.87883	2.33860
$p(F = f \mid K_R = k_R^O, K_T = k_T^O)$	$2e - 6$	0.00001	0.00030	0.00297	0.20830	0.52895	0.25529	0.00416

TABLE A2: Calculated likelihood and posterior values for worked example, across all simulated forcing levels. The evidence, or the denominator of Eq. A1, is equal to 1.88543. These values include some rounding error due to truncating numbers for publication.



## References

- Allen, M. R., and P. A. Stott, 2003: Estimating signal amplitudes in optimal fingerprinting, Part I: Theory. *Climate Dynamics*, **21** (5), 477–491, <https://doi.org/10.1007/s00382-003-0313-9>.
- Arnell, N. W., J. A. Lowe, A. J. Challinor, and T. J. Osborn, 2019: Global and regional impacts of climate change at different levels of global temperature increase. *Climatic Change*, **155**, 377–391, <https://doi.org/10.1007/s10584-019-02464-z>.
- Berliner, L. M., R. A. Levine, and D. J. Shea, 2000: Bayesian climate change assessment. *Journal of Climate*, **13** (21), 3805–3820, [https://doi.org/10.1175/1520-0442\(2000\)013\(3805:BCCA\)2.0.CO;2](https://doi.org/10.1175/1520-0442(2000)013(3805:BCCA)2.0.CO;2).
- Bonfils, C., and Coauthors, 2008: Detection and Attribution of Temperature Changes in the Mountainous Western United States. *Journal of Climate*, **21** (23), 6404–6424, <https://doi.org/10.1175/2008JCLI2397.1>.
- Bonfils, C. J. W., B. D. Santer, J. C. Fyfe, K. Marvel, T. J. Phillips, and S. R. H. Zimmerman, 2020: Human influence on joint changes in temperature, rainfall and continental aridity. *Nature Climate Change*, **10**, 726–731, <https://doi.org/10.1038/s41558-020-0821-1>.
- Brown, H. Y., B. Wagman, D. Bull, K. Peterson, B. Hillman, X. Liu, Z. Ke, and L. Lin, 2024: Validating a microphysical prognostic stratospheric aerosol implementation in e3smv2 using the mount pinatubo eruption. *EGUsphere*, **2024**, 1–46, <https://doi.org/10.5194/egusphere-2023-3041>.
- Browning, K. A., and Coauthors, 1992: Environmental Effects From Burning Oil Wells in the Gulf. *Weather*, **47** (6), 201–212, <https://doi.org/10.1002/j.1477-8696.1992.tb07162.x>.
- Callahan, C. W., and J. S. Mankin, 2022: Globally unequal effect of extreme heat on economic growth. *Science Advances*, **8** (43), <https://doi.org/10.1126/sciadv.add3726>.
- Church, J. A., N. J. White, and J. M. Arblaster, 2005: Significant decadal-scale impact of volcanic eruptions on sea level and ocean heat content. *Nature*, **438** (7064), 74–77, <https://doi.org/10.1038/nature04237>.

- Ehrmann, T., and Coauthors, 2024: Identifying Northern Hemisphere Temperature Responses to the Mt. Pinatubo Eruption through Limited Variability Ensembles, in preparation.
- Eyring, V., and Coauthors, 2021: Human Influence on the Climate System: Contribution of Working Group I to the Sixth Assessment Report of the Intergovernmental Panel on Climate Change. Tech. rep., IPCC Sixth Assessment Report.
- Gillett, N., A. Weaver, F. Zwiers, and M. Wehner, 2004: Detection of volcanic influence on global precipitation. *Geophysical Research Letters*, **31** (12), <https://doi.org/10.1029/2004GL020044>.
- Golaz, J.-C., and Coauthors, 2022: The DOE E3SM Model Version 2: Overview of the Physical Model and Initial Model Evaluation. *Journal of Advances in Modeling Earth Systems*, **14** (12), <https://doi.org/10.1029/2022MS003156>.
- Gonzalez, A., J. M. Chase, and M. I. O'Connor, 2023: A framework for the detection and attribution of biodiversity change. *Philosophical Transactions of the Royal Society B: Biological Sciences*, **378** (1881), <https://doi.org/10.1098/rstb.2022.0182>.
- Greenwald, R., M. Bergin, J. Xu, D. Cohan, G. Hoogenboom, and W. Chameides, 2006: The influence of aerosols on crop production: A study using the CERES crop model. *Agricultural Systems*, **89** (2-3), 390–413, <https://doi.org/10.1016/j.agsy.2005.10.004>.
- Gu, L., D. D. Baldocchi, S. C. Wofsy, J. W. Munger, J. J. Michalsky, S. P. Urbanski, and T. A. Boden, 2003: Response of a deciduous forest to the Mount Pinatubo eruption: Enhanced photosynthesis. *Science*, **299** (5615), 2035–2038, <https://doi.org/10.1126/science.1078366>.
- Guo, S., G. J. Bluth, W. I. Rose, I. M. Watson, and A. Prata, 2004: Re-evaluation of SO<sub>2</sub> release of the 15 June 1991 Pinatubo eruption using ultraviolet and infrared satellite sensors. *Geochemistry, Geophysics, Geosystems*, **5** (4), <https://doi.org/10.1029/2003GC000654>.
- Hannart, A., 2016: Integrated optimal fingerprinting: Method description and illustration. *Journal of Climate*, **29** (6), 1977–1998, <https://doi.org/10.1175/JCLI-D-14-00124.1>.
- Hasselmann, K., 1993: Optimal Fingerprints for the Detection of Time-dependent Climate Change. *Journal of Climate*, **6** (10), 1957–1971, [https://doi.org/10.1175/1520-0442\(1993\)006<1957:OFFTDO>2.0.CO;2](https://doi.org/10.1175/1520-0442(1993)006<1957:OFFTDO>2.0.CO;2).

- Hasselmann, K., 1997: Multi-pattern fingerprint method for detection and attribution of climate change. *Climate Dynamics*, **13** (9), 601–611, <https://doi.org/10.1007/s003820050185>.
- Hegerl, G. C., K. Hasselmann, U. Cubasch, J. F. Mitchell, E. Roeckner, R. Voss, and J. Waszkewitz, 1997: Multi-fingerprint detection and attribution analysis of greenhouse gas, greenhouse gas-plus-aerosol and solar forced climate change. *Climate Dynamics*, **13** (9), 613–634, <https://doi.org/10.1007/s003820050186>.
- Hegerl, G. C., O. Hoegh-Guldberg, G. Casassa, M. Hoerling, S. Kovats, C. Parmesan, D. Pierce, and P. Stott, 2010: Good practice guidance paper on detection and attribution related to anthropogenic climate change. Tech. rep., Intergovernmental Panel on Climate Change Expert Meeting on Detection and Attribution of Anthropogenic Climate Change.
- Hegerl, G. C., and G. R. North, 1997: Comparison of statistically optimal approaches to detecting anthropogenic climate change. *Journal of Climate*, **10** (5), 1125–1133, [https://doi.org/10.1175/1520-0442\(1997\)010<1125:COSOAT>2.0.CO;2](https://doi.org/10.1175/1520-0442(1997)010<1125:COSOAT>2.0.CO;2).
- Herger, N., B. M. Sanderson, and R. Knutti, 2015: Improved pattern scaling approaches for the use in climate impact studies. *Geophysical Research Letters*, **42** (9), 3486–3494, <https://doi.org/10.1002/2015GL063569>.
- Hill, S. A. B., 1965: The Environment and Disease: Association or Causation? *Proceedings of the Royal Society of Medicine*, **58** (5), 295–300, <https://doi.org/10.1177/003591576505800503>.
- Inman, H. F., and E. L. Bradley, Jr., 1989: The overlapping coefficient as a measure of agreement between probability distributions and point estimation of the overlap of two normal densities. *Communications in Statistics - Theory and Methods*, **18** (10), 3851–3874, <https://doi.org/10.1080/03610928908830127>.
- Irvine, P. J., B. Kravitz, M. G. Lawrence, and H. Muri, 2016: An overview of the Earth system science of solar geoengineering. *WIREs Climate Change*, **7** (6), 815–833, <https://doi.org/10.1002/wcc.423>.
- Kapoor, S., and A. Narayanan, 2023: Leakage and the reproducibility crisis in machine-learning-based science. *Patterns*, **4** (9), <https://doi.org/10.1016/j.patter.2023.100804>.

- Keys, P. W., E. A. Barnes, N. S. Diffenbaugh, J. W. Hurrell, and C. M. Bell, 2022: Potential for perceived failure of stratospheric aerosol injection deployment. *Proceedings of the National Academy of Sciences of the United States of America*, **119** (40), 1–8, <https://doi.org/10.1073/pnas.2210036119>.
- Kremser, S., and Coauthors, 2016: Stratospheric Aerosol–Observations, Processes, and Impact on Climate. *Reviews of Geophysics*, **54** (2), 278–335, <https://doi.org/10.1002/2015RG000511>.
- Labitzke, K., and M. P. McCormick, 1992: Stratospheric temperature increases due to Pinatubo aerosols. *Geophysical Research Letters*, **19** (2), 207–210, <https://doi.org/10.1029/91GL02940>.
- Liu, X., P.-L. Ma, H. Wang, S. Tilmes, B. Singh, R. C. Easter, S. J. Ghan, and P. J. Rasch, 2016: Description and evaluation of a new four-mode version of the Modal Aerosol Module (MAM4) within version 5.3 of the Community Atmosphere Model. *Geoscientific Model Development*, **9** (2), 505–522, <https://doi.org/10.5194/gmd-9-505-2016>.
- Liu, X., and Coauthors, 2012: Toward a minimal representation of aerosols in climate models: description and evaluation in the Community Atmosphere Model CAM5. *Geoscientific Model Development*, **5** (3), 709–739, <https://doi.org/10.5194/gmd-5-709-2012>.
- Liu, Y., S. Goodrick, and W. Heilman, 2014: Wildland fire emissions, carbon, and climate: Wildfire-climate interactions. *Forest Ecology and Management*, **317**, 80–96, <https://doi.org/10.1016/j.foreco.2013.02.020>.
- Luber, G., and M. McGeehin, 2008: Climate Change and Extreme Heat Events. *American Journal of Preventive Medicine*, **35** (5), 429–435, <https://doi.org/10.1016/j.amepre.2008.08.021>.
- Marshall, L., and Coauthors, 2019: Exploring how eruption source parameters affect volcanic radiative forcing using statistical emulation. *Journal of Geophysical Research: Atmospheres*, **124** (2), 964–985, <https://doi.org/10.1029/2018JD028675>.
- Marvel, K., M. Biasutti, and C. Bonfils, 2020: Fingerprints of external forcings on Sahel rainfall: aerosols, greenhouse gases, and model-observation discrepancies. *Environmental Research Letters*, **15** (8), 084 023, <https://doi.org/10.1088/1748-9326/ab858e>.

- Mitchell, J., D. Karoly, G. Hegerl, F. Zwiers, M. Allen, and J. Marengo, 2001: Detection of climate change and attribution of causes. Tech. rep., Intergovernmental Panel on Climate Change (IPCC), Assessment Report 3.
- National Intelligence Council, 2021: Climate Change and International Responses Increasing Challenges to US National Security Through 2040. Tech. rep.
- North, G. R., and M. J. Stevens, 1998: Detecting climate signals in the surface temperature record. *Journal of Climate*, **11** (4), 563–577, [https://doi.org/10.1175/1520-0442\(1998\)011<0563:DCSITS>2.0.CO;2](https://doi.org/10.1175/1520-0442(1998)011<0563:DCSITS>2.0.CO;2).
- Osborn, T. J., C. J. Wallace, I. C. Harris, and T. M. Melvin, 2016: Pattern scaling using ClimGen: monthly-resolution future climate scenarios including changes in the variability of precipitation. *Climatic Change*, **134** (3), 353–369, <https://doi.org/10.1007/s10584-015-1509-9>.
- Parker, D. E., H. Wilson, P. D. Jones, J. Christy, and C. K. Folland, 1996: The impact of Mount Pinatubo on world-wide temperatures. *International Journal of Climatology*, **16** (5), 487–497, [https://doi.org/10.1002/\(SICI\)1097-0088\(199605\)16:5<487::AID-JOC39>3.0.CO;2-J](https://doi.org/10.1002/(SICI)1097-0088(199605)16:5<487::AID-JOC39>3.0.CO;2-J).
- Proctor, J., S. Hsiang, J. Burney, M. Burke, and W. Schlenker, 2018: Estimating global agricultural effects of geoengineering using volcanic eruptions. *Nature*, **560** (7719), 480–483, <https://doi.org/10.1038/s41586-018-0417-3>.
- Ramachandran, S., V. Ramaswamy, G. L. Stenchikov, and A. Robock, 2000: Radiative impact of the Mount Pinatubo volcanic eruption: Lower stratospheric response. *Journal of Geophysical Research: Atmospheres*, **105** (D19), 24 409–24 429, <https://doi.org/10.1029/2000JD900355>.
- Ribes, A., S. Planton, and L. Terray, 2013: Application of regularised optimal fingerprinting to attribution. Part I: method, properties and idealised analysis. *Climate Dynamics*, **41** (11), 2817–2836, <https://doi.org/10.1007/s00382-013-1735-7>.
- Richter, J. H., and Coauthors, 2022: Assessing Responses and Impacts of Solar climate intervention on the Earth system with stratospheric aerosol injection (ARISE-SAI): protocol and initial results from the first simulations. *Geoscientific Model Development*, **15** (22), 8221–8243, <https://doi.org/10.5194/gmd-15-8221-2022>.

- Rieger, L. A., J. N. Cole, J. C. Fyfe, S. Po-Chedley, P. J. Cameron-Smith, P. J. Durack, N. P. Gillett, and Q. Tang, 2020: Quantifying CanESM5 and EAMv1 sensitivities to Mt. Pinatubo volcanic forcing for the CMIP6 historical experiment. *Geoscientific Model Development*, **13** (10), 4831–4843, <https://doi.org/10.5194/gmd-13-4831-2020>.
- Robock, A., 2000: Volcanic eruptions and climate. *Reviews of Geophysics*, **38** (2), 191–219, <https://doi.org/10.1029/1998RG000054>.
- Santer, B., T. Wigley, and P. Jones, 1993: Correlation methods in fingerprint detection studies. *Climate Dynamics*, **8** (6), 265–276, <https://doi.org/10.1007/BF00209666>.
- Santer, B. D., and Coauthors, 2011: Separating signal and noise in atmospheric temperature changes: The importance of timescale. *Journal of Geophysical Research: Atmospheres*, **116** (D22), <https://doi.org/10.1029/2011JD016263>.
- Santer, B. D., and Coauthors, 2014: Volcanic contribution to decadal changes in tropospheric temperature. *Nature Geoscience*, **7** (3), 185–189, <https://doi.org/10.1038/ngeo2098>.
- Smith, A. B., and R. W. Katz, 2013: US billion-dollar weather and climate disasters: Data sources, trends, accuracy and biases. *Natural Hazards*, **67**, 387–410, <https://doi.org/10.1007/s11069-013-0566-5>.
- Soden, B. J., R. T. Wetherald, G. L. Stenchikov, and A. Robock, 2002: Global cooling after the eruption of Mount Pinatubo: A test of climate feedback by water vapor. *Science*, **296** (5568), 727–730, <https://doi.org/10.1126/science.296.5568.727>.
- Stott, P. A., N. P. Gillett, G. C. Hegerl, D. J. Karoly, D. A. Stone, X. Zhang, and F. Zwiers, 2010: Detection and attribution of climate change: a regional perspective. *Wiley Interdisciplinary Reviews: Climate Change*, **1** (2), 192–211, <https://doi.org/10.1002/wcc.34>.
- Wills, R. C. J., D. S. Battisti, K. C. Armour, T. Schneider, and C. Deser, 2020: Pattern Recognition Methods to Separate Forced Responses from Internal Variability in Climate Model Ensembles and Observations. *Journal of Climate*, **33** (20), 8693–8719, <https://doi.org/10.1175/JCLI-D-19-0855.1>.
- Yamamoto, L., and M. Esteban, 2010: Vanishing Island States and sovereignty. *Ocean and Coastal Management*, **53**, 1–9, <https://doi.org/10.1016/j.ocecoaman.2009.10.003>.

Zanchettin, D., and Coauthors, 2022: Effects of forcing differences and initial conditions on inter-model agreement in the VolMIP volc-pinatubo-full experiment. *Geoscientific Model Development*, **15** (5), 2265–2292, <https://doi.org/10.5194/gmd-15-2265-2022>.

# Supplement: Conditional multi-step attribution for climate forcings

Christopher R. Wentland<sup>1</sup>, Michael Weylandt<sup>2</sup>, Laura P. Swiler<sup>3</sup>, Thomas S. Ehrmann<sup>3</sup>, and Diana Bull<sup>3</sup>

<sup>1</sup>Sandia National Laboratories, Livermore, CA, USA

<sup>2</sup>Zicklin School of Business, Baruch College, CUNY, New York, NY, USA

<sup>3</sup>Sandia National Laboratories, Albuquerque, NM, USA

## Linear regression fits for single-step pathways

In the paper body, we compared the proposed multi-step pathways to the associated single-step pathways, i.e., those which predict a temperature change directly from the source forcing magnitude. These exclude the intermediate radiative flux variables, and were shown to perform poorly in correctly attributing the “observed” 10 Tg forcing. The linear regression fits associated with these single-step pathways are provided in Figure 1. While the single-step stratosphere warming pathway is strongly correlated, with an  $R^2$  value of 0.95, the single-step surface cooling pathway exhibits much greater variance, resulting in an  $R^2$  value of approximately 0.62. This no doubt lends to the poor attribution results associated with the single-step surface cooling posteriors, and further explains why the combined single-step pathway provides very little improvement over the single-step stratosphere warming pathway.

## Posteriors under volcano-agnostic prior

In the paper body, two prior sets were used to assess the sensitivity of the attribution posteriors to the prior distribution: a well specified prior and a poorly specified prior. As a somewhat contrived experiment, we may also specify a “volcano-agnostic” prior, signifying a situation in which it is not known that a volcano has erupted and operates under a general understanding that volcanic eruptions are extremely uncommon. This prior is detailed in Table 1: a large prior probability is placed on the counterfactual 0 Tg scenario, while all other forcing levels are assigned a very small prior probability. One might think of this as representative of a scenario where independent actors surreptitiously engage in geoengineering projects, such as stratospheric aerosol injection. Again, this prior set is rather artificial, but provides another data point for the sensitivity of the proposed multi-step attribution method to the prior distribution.

The resulting posterior distributions under the volcano-agnostic prior are displayed in Figure 2. As with the well specified prior, the stratosphere warming pathways in Figure 2a



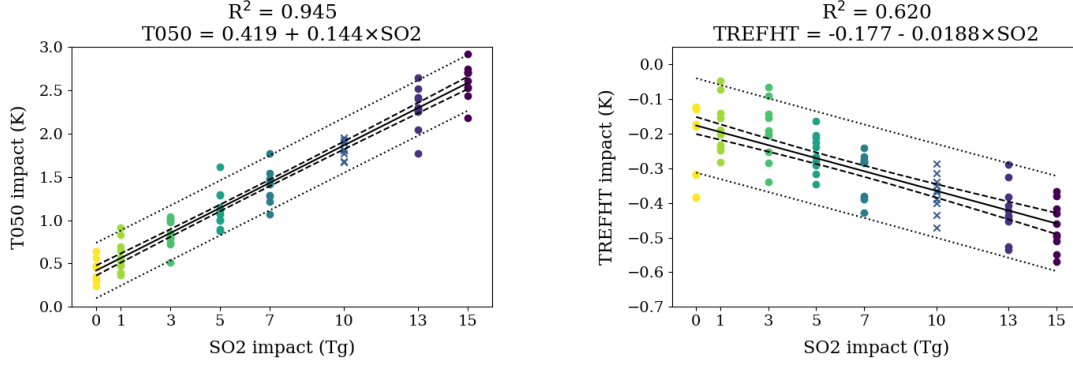
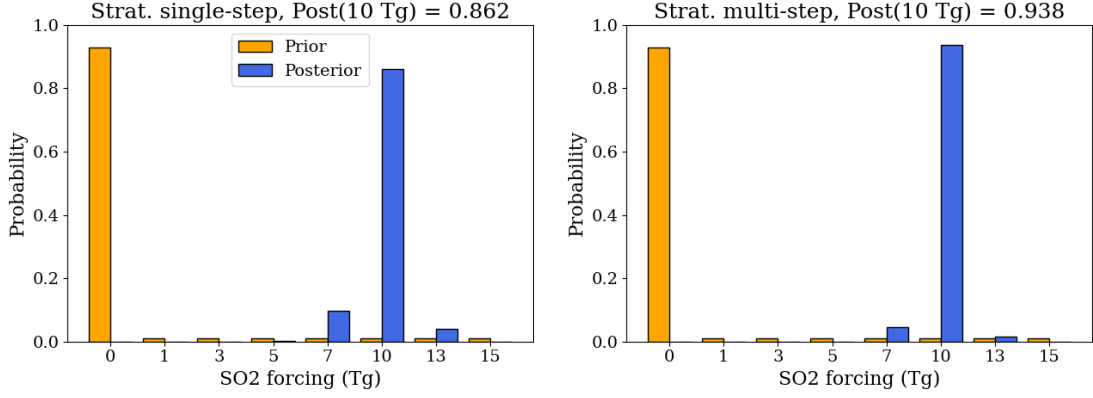


Figure 1: Global average impact linear regression fits for single-step stratosphere warming pathway (left) and surface cooling pathway (right). These include the OLS fit (solid line), 90% confidence interval (dashed line), and 90% prediction interval (dotted line). Linear model parameters and  $R^2$  values are noted in the figure titles. The 10 Tg data are not included in computing the regression, and are marked separately on the plots.

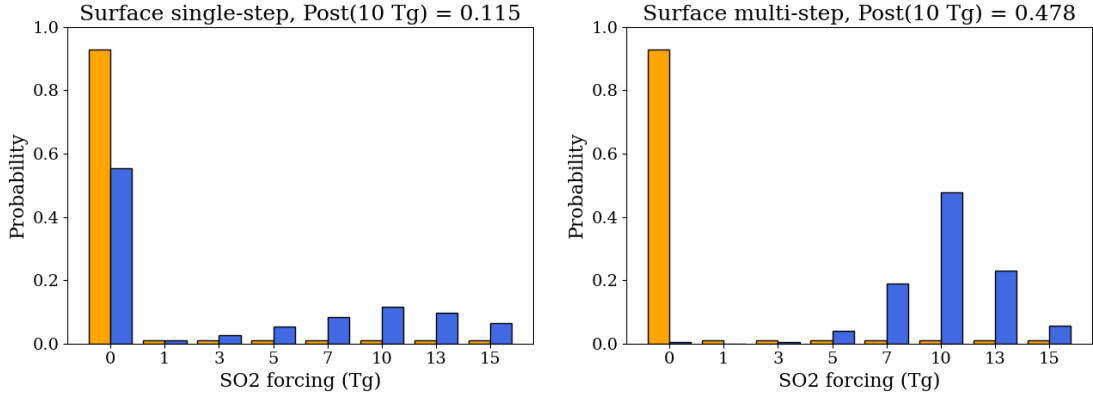
Prior set	0 Tg	1 Tg	3 Tg	5 Tg	7 Tg	10 Tg	13 Tg	15 Tg
Volcano-agnostic	0.93	0.01	0.01	0.01	0.01	0.01	0.01	0.01

Table 1: Prior probabilities for simulated forcing levels.

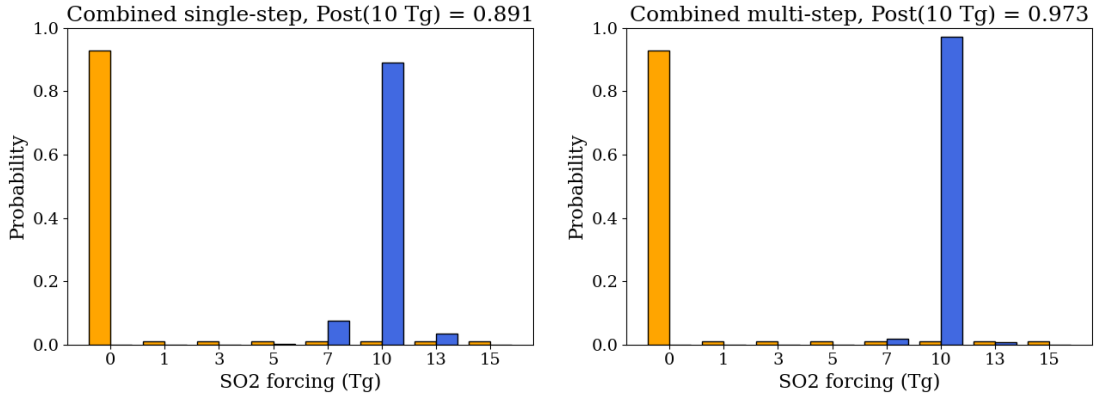
results in high confidence in correctly attributing the 10 Tg forcing, even under the single-step pathway. This contrasts with the poorly specified prior, where weighting the 7 Tg forcing results in incorrect or highly uncertain attribution for the stratosphere warming pathway. Under the surface warming pathway in Figure 2b, however, the single-step pathway incorrectly identifies the counterfactual scenario as the most likely. However, the multi-step surface cooling pathway correctly identifies the 10 Tg forcing as at least two times more likely than any other forcing despite the large prior on the counterfactual. This provides yet more evidence that including intermediate variables in the pathway improves attribution quality. The combined pathway in Figure 2c provides marginal improvement over the stratosphere warming pathway, effectively halving the uncertainty in correctly attributing the 10 Tg forcing under the multi-step pathway.



(a) Stratosphere warming pathway.



(b) Surface cooling pathway.



(c) Combined pathway.

Figure 2: Posterior probabilities (blue) under volcano-agnostic prior distribution (orange), for stratosphere warming only (top), surface cooling only (middle) and combined pathways (bottom), for single-step (left) and multi-step (right) pathways. The 10 Tg posterior is noted in the figure titles.